aerospace

MDPI

Article

Study of a Regional Turboprop Aircraft with Electrically Assisted Turboshaft

Anaïs Luisa Habermann *, **Moritz Georg Kolb**, **Philipp Maas**, **Hagen Kellermann**, **Carsten Rischmüller**, **Fabian Peter** and **Arne Seitz**

Bauhaus Luftfahrt e.V., Willy-Messerschmitt-Str. 1, 82024 Taufkirchen, Germany; moritz.kolb@bauhaus-luftfahrt.net (M.G.K.); philipp.maas@bauhaus-luftfahrt.net (P.M.); hagen.kellermann@bauhaus-luftfahrt.net (H.K.); carsten.rischmueller@bauhaus-luftfahrt.net (C.R.); fabian.peter@bauhaus-luftfahrt.net (F.P.); arne.seitz@bauhaus-luftfahrt.net (A.S.)

* Correspondence: anais.habermann@bauhaus-luftfahrt.net

Abstract: Hybrid-Electric Propulsion (HEP) could be part of the solution to decrease emissions associated with regional commercial aviation. This study presents results for the aircraft level fuel reduction potential of a regional turboprop concept with an HEP architecture and Entry-Into-Service (EIS) in 2035+. The configuration specifically tackles the elaborated challenges of introducing an additional electrical energy source to the configuration by employing a twofold electrical assistance to a turboshaft engine in combination with an innovative thermal management concept. Relevant components and disciplines were modeled and incorporated into an integrated aircraft design environment. The behavior and interaction of the HEP architecture with the aircraft was thoroughly investigated. A best-performing configuration was derived and compared with a conventional reference configuration following a State-of-the-Art (SoA) reference aircraft approach. For a typical mission with 200 nmi range, a block fuel reduction of 9.6% was found. However, the assumed battery performance characteristics limited the reduction potential and led to a fuel burn increase for the 600 nmi design mission. Furthermore, sourcing the non-propulsive subsystems directly from the on-board battery was detrimental. The innovative Thermal Management System (TMS) located in the propeller slipstream showed a synergistic effect with the investigated configuration.

Keywords: regional aircraft; (conceptual) aircraft design; hybrid-electric propulsion; parallel-hybrid propulsion; cycle-integrated parallel hybrid; mechanically integrated parallel hybrid; hybridization strategy; thermal management system; IMOTHEP

Citation: Habermann, A.L.; Kolb, M.G.; Maas, P.; Kellermann, H.; Rischmüller, C.; Peter, F.; Seitz, A. Study of a Regional Turboprop Aircraft with Electrically Assisted Turboshaft. *Aerospace* **2023**, *10*, 529. https://doi.org/10.3390/aerospace10060529

Academic Editor: Jae Hyun Park

Received: 2 May 2023
Revised: 17 May 2023
Accepted: 19 May 2023
Published: 2 June 2023

1. Introduction

Due to the apparent need to reduce the impact of aviation on climate change, the electrification of aircraft as an enabler for low-emission air transportation has been increasingly studied in recent years (see, for example, [1–5]). For short ranges, the fuel reduction potential is higher for low battery gravimetric energy densities, which can be expected in the near future, compared with longer ranges [2]. Thus, HEP is deemed most suited for market segments with short design and operational ranges, such as regional air transportation (e.g., [2,3,5,6]). Following the successful flight of early CS-23 prototypes, regional turboprop application is a likely first step to a global electrification of commercial aviation through CS-25-type aircraft [7].

For design mission ranges typical to regional aircraft, HEP is, thus, a promising technology. Several studies are focusing on investigating the potential of regional HEP aircraft configurations, such as the projects PEGASUS (Parallel Electric-Gas Architecture with Synergistic Utilization Scheme) [8], IRON (Innovative turbopROp configuratioN) [7], HECARRUS (Hybrid ElectriC smAll commuteR aiRcraft conceptUal deSign) [9], FutPrInt50 (Future Propulsion and Integration: towards a hybrid-electric 50-seat regional aircraft) [10] and the studies presented in [6,11–15]. Most investigated configurations are based on the

ATR (Avions de Transport Régional) 42 or ATR 72 aircraft, employing different combinations of technologies in addition to a hybrid-electric power train. These include distributed electric propulsion, boundary layer ingestion and blown wings.

For all configurations, the usage of electrical energy can contribute to an overall emission reduction if the aircraft configuration adequately addresses the challenges of HEP. HEP poses two major challenges: flight performance degradation on the aircraft level due to cascade effects, which are primarily caused by the additional weight of batteries and electrical components (especially due to the disadvantageous gravimetric energy density of the batteries), and the handling of significant excessive waste heat attributed to the same components.

The presented methodology and results are part of the European-Union-funded Horizon 2020 IMOTHEP project (Investigation and Maturation of Technologies for Hybrid-Electric Propulsion) following a holistic aircraft design approach [16]. The project aims at identifying the potential benefits of HEP to reduce commercial aircraft emissions by conducting in-depth analyses of power train technologies in combination with innovative propulsion architectures [16]. Two regional and two short-to-medium range aircraft configurations with HEP are investigated with increasing levels of detail and fidelity in a three-step process (L0–L2).

This study presents the integrated aircraft level results of the second conceptual aircraft design loop (L1) for one of the regional platforms identified as REG-CON (REGional-CONservative) in IMOTHEP. Its results will be incorporated in the European roadmap toward HEP resulting from the project.

The aircraft concept investigated in this study combines technologies which shall offer a solution to the elaborated challenges for a hybrid-electric regional turboprop aircraft with an EIS in 2035+. It combines a flexible utilization of electrical energy in an advanced parallel-hybrid power plant architecture [17] with propeller slipstream-enhanced electrical waste heat rejection through wing surface heat exchangers [18].

The studied configuration is based on a twin-turboshaft propulsion architecture with two propellers (similar to the existing ATR 42-600), which features electrical assistance to the turboshaft engines. The required electrical energy is sourced from an on-board battery system.

To gain a thorough understanding of the impact of such an HEP configuration, all required components and disciplines are represented by detailed models and methods. A special focus is placed on the modeling of the electrically assisted turbo generator (see also [17]), the battery (see also [19]) and the hybrid-electric power train.

To contrast the fuel demand of the proposed aircraft configuration against a conventionally evolved configuration with the same EIS, aircraft level results for a typical mission of the hybrid-electric aircraft are compared against the performance of a reference aircraft with similar Top-Level Aircraft Requirements (TLARs). The reference aircraft is derived from the ATR 42-600 using an evolutionary projection for the advances in conventional structural, aerodynamic and propulsive technologies to the year 2035+. In addition, sensitivity study results are analyzed to improve the understanding of the impact of key technology performance parameters on the potential of HEP for the regional turboprop configuration.

2. Regional Turboprop Configuration with Twofold Electrical Assistance

TLARs, which were deemed suitable for an EIS 2035+ HEP aircraft, were derived for the regional aircraft investigated in IMOTHEP. They were employed for the SoA reference aircraft approach to evaluate the fuel burn reduction potential of the HEP configuration.

2.1. Top Level Aircraft Requirements

Table 1 summarizes the project-specific TLARs for the regional configurations. They were applied to all reference and HEP configurations. The "Typical Mission" (200 nmi, Ma_{cruise} 0.40, FL150) served as the reference mission for mission fuel burn estimation.

Table 1. Project-specific Top Level Aircraft Requirements.

TLAR	Value
EIS	2035+
Standard design capacity [1]	40 seats @ 33.6″ seat pitch
Maximum design capacity [1]	48 seats @ 28.0″ seat pitch
Aisle/seat width	19.0″/18.0″
Cabin height	2 m
Design/typical range (std. layout, high-speed cruise)	600 nmi/200 nmi
Maximum cruise speed FL 150, ISA	245 kts–300 kts (Ma 0.40)
OEI ceiling @ISA+10/AEO ceiling @ISA	FL150/FL200–250
TOFL @SL, ISA, MTOM, dry concrete runways	≤1100 m
TODA @5400 ft, ISA+30, TOM (typical mission @300 nmi), dry concrete runways (take-off from Denver airport)	≤3658 m
LFL @SL, ISA, MLM, dry concrete runways	≤1100 m
Time to climb from 1500 ft to FL150 @MTOM, ISA	≤13 min
Turnaround time	≤20 min

[1] 106 kg/PAX.

2.2. Reference Aircraft Approach

As depicted in Figure 1, the ATR 42-600 aircraft (i.e., REG-REFX) was employed to calibrate the handbook methods used for the estimation of aircraft aerodynamics, weights and the turboshaft model similar to the PW127M. Based on the REG-REFX, the REG-REF was derived, which features the same technology scenario as the REG-REFX, but is based on the project-specific TLARs.

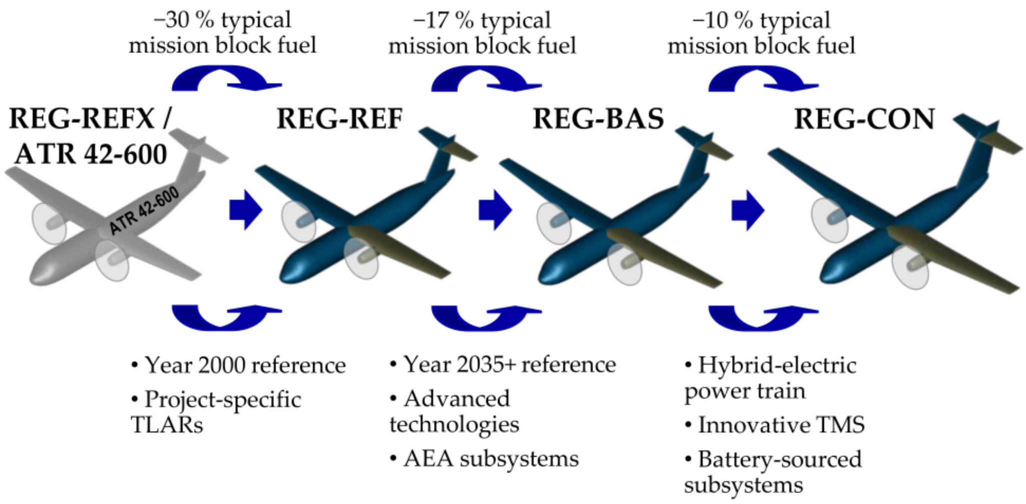

Figure 1. Reference aircraft approach.

The REG-BAS served as the main reference aircraft. It is a projection of a conventional aircraft configuration to the year 2035+. It was derived from the REG-REF by assuming evolutionary technology advancements of all components, including the turboshaft. The technology assumptions are summarized in Table 2.

To arrive at the REG-CON configuration, the gas turbine architecture of the REG-BAS was replaced by the configuration-specific HEP architecture, batteries were added as a second energy source and all additional adaptions to the aircraft, which were related to the changed propulsion architecture, were considered. In addition, the non-propulsive subsystems were sourced from the on-board battery.

Table 2. Technology assumptions for the year 2035+.

Discipline	Component	Technology/Improvement Measure	Affected Parameter
Aerodynamics	Wing	Increased aspect ratio (from 11 to 14)	Induced drag
Weights	Fuselage	Fully composite and advanced bonding technologies	Fuselage structural weight: −7%
Weights	Wing	90% composites, advanced materials and bonding technologies, additive manufacturing	Wing structural weight: −10%
Weights	Empennage	Increased use of composites, advanced bonding technologies	Empennage structural weight: −8%
Weights	Furnishing and standard items	Advanced lightweight materials, additive manufacturing	Furnishing and standard items structural weight: −20%
Weights	Landing gear	Increased use of composites	Landing gear structural weight: −5%
Weights	Turbo engine	Engine power-to-weight ratio	Dry engine weight: −13%
Propulsion	Turbo engine	Increased thermal efficiency	PSFC: −14%
Weights	Non-prop. Subsystems	More-electric subsystems	Subsystems weight
Power	Non-prop. Subsystems	More-electric subsystems	Power off-takes

2.3. Hybrid-Electric Propulsion Configuration

The REG-CON is based on a twin-turboshaft propulsion architecture with two propellers, which feature electrical assistance from batteries to the turboshaft engines. The electrical assistance is twofold: Cycle-Integrated Parallel Hybrid electrical assistance—CIPH [18], i.e., an electrically assisted compressor, is combined with a Mechanically Integrated Parallel Hybrid—MIPH [20], i.e., electrical assistance to the power shaft.

Furthermore, the concept features an unconventional electric waste heat management system, which rejects heat over the wetted surfaces of the aircraft [21].

A visualization of the REG-CON aircraft concept is presented in Figure 2.

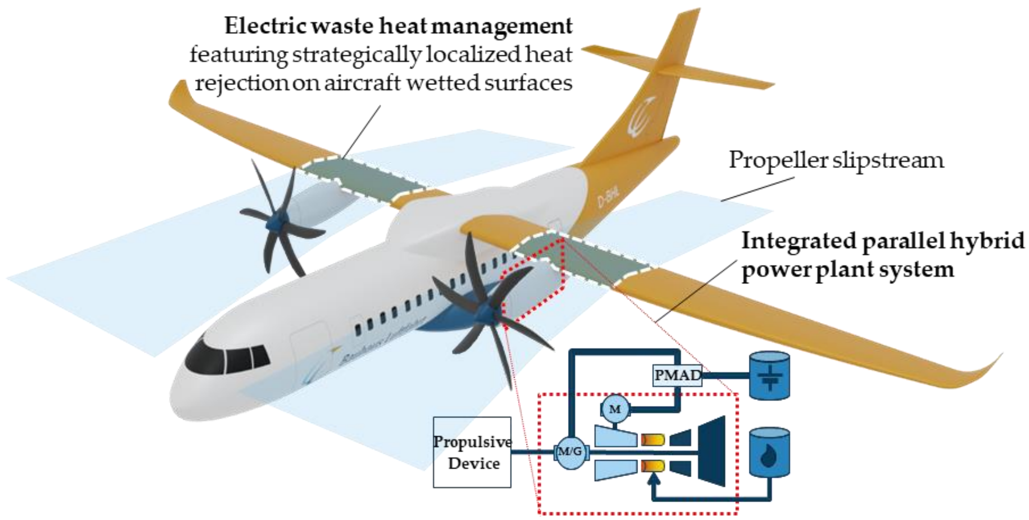

Figure 2. Visualization of the REG-CON aircraft configuration. Source: [22].

The energy for the REG-CON propulsion system is provided by battery packs located within the enlarged belly fairing as well as by fuel stored in the integral tanks of the wings. Depending on the degree of power hybridization (H_P, see Equation (1)) and the power split (S_P, see Equation (2)), electric power directed from the battery to an electric machine attached to the power shaft prior to the propeller gearbox is added to the power generated by the power shaft of the turboprop engine. Furthermore, the turboprop engine is enhanced to a CIPH engine by providing varying amounts of electrical assistance to the High-Pressure Compressor (HPC) via an electric motor, delivered through a tower shaft. The general layout of the electrically enhanced propulsion system is depicted in Figure 3.

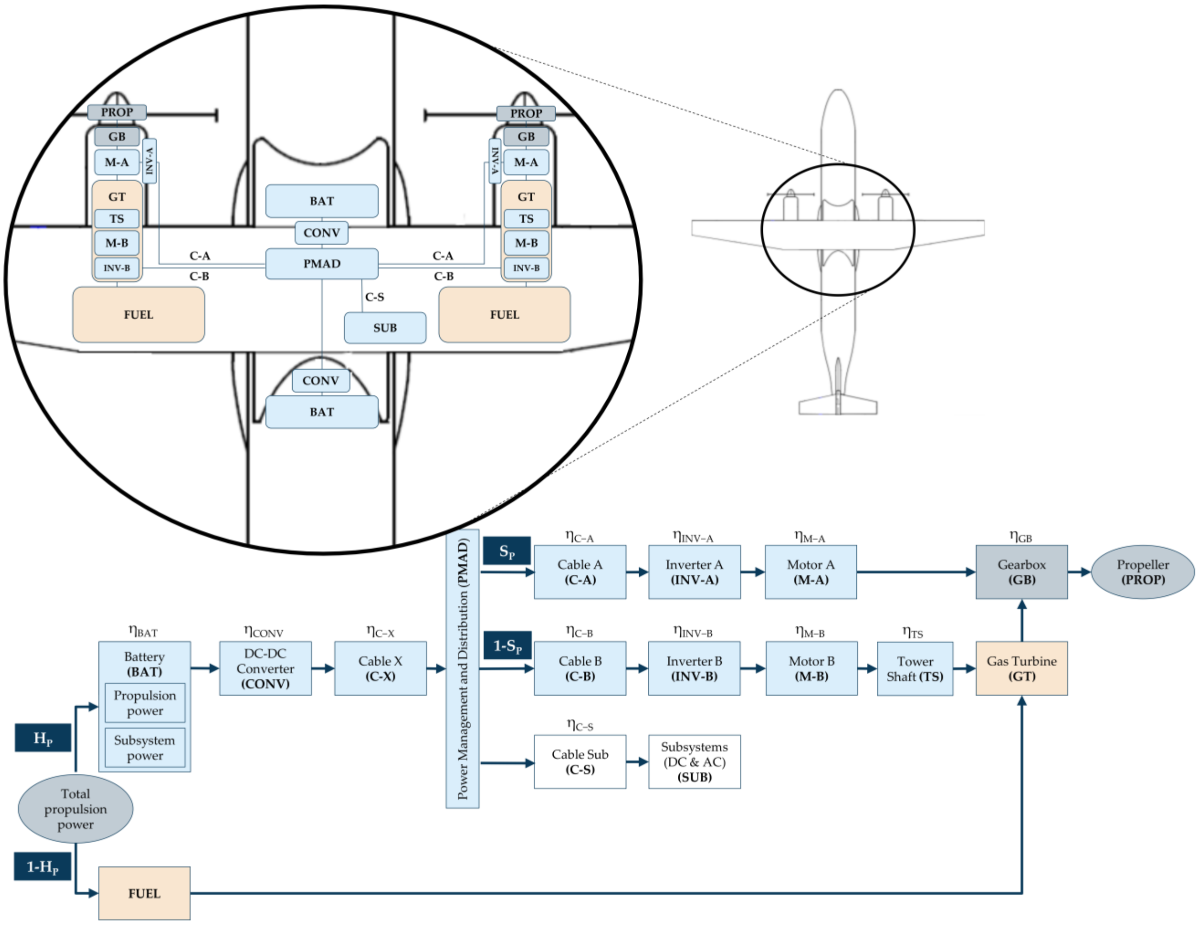

Figure 3. Positioning of HEP components inside the aircraft and simplified HEP load flow scheme.

The central element of the hybrid-electric system is the power distribution unit. Here, the electric battery power is directed to the four electric motors (two for each propulsion unit) as well as the non-propulsive subsystems according to the requirements and the desired S_P. The use of power instead of energy for the derivation of the hybridization degree H_P and power split S_P includes conversion losses and, thus, facilitates the calculation process. According to, e.g., Seitz et al. [20], H_P is the ratio of electric supply power $P_{sup,el}$ to the total supply power $P_{sup,tot}$:

$$H_P = \frac{P_{sup,el}}{P_{sup,tot}} = \frac{P_{bat,prop}}{P_{bat,prop}+P_{fuel}} \tag{1}$$

In this case, $P_{bat,prop}$ is the electrical supply power, which is required to feed the electric machine of the hybrid power shaft drive (motor A) and the high-pressure compressor drive (motor B). P_{fuel} is the fuel power supplied to the thermal engine. In addition, the battery has to supply power to the non-propulsive subsystem, $P_{bat,sub}$.

S_P is defined as the ratio of power supplied to the electrical assistance of the power shaft (motor A) and the total electrical power supplied to motor A and motor B:

$$S_P = \frac{P_{el,A}}{P_{el,tot}} = \frac{P_{el,A}}{P_{el,A}+P_{el,B}} \tag{2}$$

The layout of the electrically assisted turboshaft engine features a three-spool architecture, where the CIPH system provides electrical assistance to the High-Pressure (HP) spool. The electric drive is integrated via the tower shaft placed ahead of the centrifugal compressor to alleviate spatial and mechanical complexity regarding this integration position. Thanks to the higher rotational speed of the HP spool, the concept yields a light and compact electric motor and small system weight. In terms of system efficiency, it features low flow path and mechanical losses, as no electrical wiring is needed to be routed through the flow path. Furthermore, the three-spool turboshaft layout featuring a power shaft is expected to improve system operational behavior, allowing for higher operational flexibility and higher H_P. Together with the mechanically integrated system driving the power shaft, the concept of the electrically assisted turboshaft engine is depicted in Figure 4. Further details on the engine architecture can be found in [17].

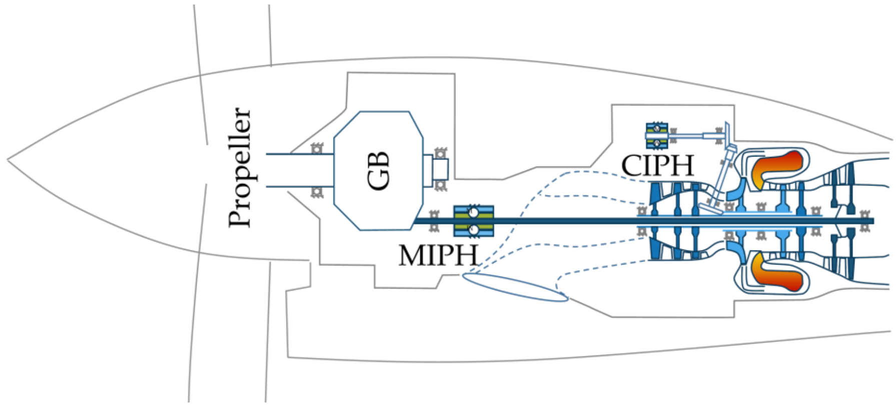

Figure 4. Concept sketch of the electrically assisted turboshaft configuration.

In order to serve as an adequate additional or alternative energy source for aircraft propulsion, batteries, which are used as an on-board energy source, need to fulfil a number of technical requirements. From a certification and safety perspective, they need to be reliable and it must be possible to contain threats to the safety of the passengers and the aircraft with reasonable effort. To prevent detrimental cascade effects in aircraft performance, the gravimetric energy and/or power density of the battery cell and pack needs to be as high as possible. Furthermore, if the batteries can be operated at high temperatures, the heat loads can be minimized and the TMS can be smaller in size and weight.

Current research on solid-state batteries promises to fulfil the specified requirements in the future. However, as the advances in solid-state battery technology are not yet promising for market readiness in 2035+, it was decided to employ hybrid Li-Metal batteries within the IMOTHEP project [18]. Compared with Li-Ion batteries, which are currently used in automotive applications, hybrid Li-Metal batteries provide a higher safety as they are chemically more stable and less flammable. Additionally, they feature higher gravimetric energy and power densities, they can be operated at higher operating temperatures and have an improved cycle life [23].

It was assumed that two battery bays are located closely in front of and behind the aircraft's Center of Gravity (CoG) inside an enlarged belly fairing, which provides the potential to tailor the distribution of the batteries according to the CoG requirement. Furthermore, this option allows for a higher battery growth potential, i.e., higher H_P is admissible. In addition, the design of most aircraft components remains largely unaffected, while only a minor belly fairing and fuselage weight and drag increase has to be considered. During operation, a CoG adaption between flights could also be feasible for this option. Furthermore, it potentially allows for a reconfiguration of the aircraft by reducing the number of battery packs for different application cases, i.e., different typical missions, to further reduce typical mission fuel burn. Locating the battery bays at a distance from each other in front of and behind the body landing gear meets the safety requirement for a zonal separation of the energy sources. However, the selected battery position option poses several challenges to the battery bay design. Special containment will be required against safety issues in case of landing gear failure during landing and in case of rotor burst.

The thermal household of the REG-CON hybrid-electric propulsion system and the overall aircraft is controlled by an innovative TMS. Generally, a TMS adds mass and drag to the aircraft and requires additional power. A broad variety of options for the TMS architecture exists that have been investigated for HEP application cases. These include a TMS with compact Ram-air Heat EXchangers (R-HEXs) [24] as well as TMSs with Surface Heat EXchangers (S-HEXs) [21,25]. The R-HEX has a theoretically infinite scalability regarding the possible heat transfer rate. Through its compactness, maintenance is less of a challenge and the location inside a closed air duct allows greater operational flexibility, such as through the installation of a puller tractor fan. The S-HEX can only use the existing aircraft surfaces. Thus, there is a theoretical limit to its heat transfer rate. The integration into the existing airframe can be drag-free or even aerodynamically beneficial [25], and there may be weight savings compared with an R-HEX, if parts of the S-HEX's structure can also carry loads.

For the REG-CON, both TMS solutions were considered and investigated. The objective was to find a TMS that reliably removes all waste heat of the propulsion power train and non-propulsive subsystems and, at the same time, has the least negative impact on the aircraft's performance. A particular disadvantage of the S-HEX is the limited heat transfer rate in low-speed operating points [21]. The REG-CON aircraft concept was therefore intended to utilize the slipstream of the installed propellers in order to augment heat transfer across the wetted external surface areas of the wing, especially during critical mission phases such as take-off, go-around and taxi-in (see Figure 2).

3. Aircraft Design Methodology

The integrated sizing process included the setup of an integrated sizing environment, the incorporation of all component and system models and the definition of important design laws. Details on the models and their integration in the framework are presented in the following.

3.1. Integrated Sizing Environment

The integrated sizing environment employed in this study is based on the aircraft design framework BLADE (Bauhaus Luftfahrt Aircraft Design Environment). BLADE is a modular aircraft design and sizing framework developed in-house at BHL (Bauhaus Luftfahrt e.V.). It is based on the programming language Python and employs the open source data exchange format CPACS (Common Parametric Aircraft Configuration Schema) [26] for data exchange between the modules.

The framework architecture is fully modular and allows for an aircraft configuration and study-specific setup of modules (such as geometry, weights, aerodynamics, propulsion system, etc.) including zooming capability in order to increase the level of analysis detail as required for a given study. For the presented studies, the toolchain setup depicted in Figure 5 was employed.

Fuselage geometry, TLARs, technology assumptions, required missions, hybridization strategies and specific settings for all tools were defined in an initial CPACS file, which served as an input to the toolchain. A loop driver module ensured that the toolchain was run in an iterative manner until all convergence criteria were met under the given constraints. The aircraft geometry served as an input to the weight and aerodynamics estimation modules. Both are based on handbook methods used for conceptual aircraft design, such as semi-empirical relations for conventional commercial aircraft introduced by Torenbeek [27] and Raymer [28]. Additional semi-empirical and aerodynamic estimation methods were calibrated to the ATR 42-600 aircraft configuration. Based on the calibration, the REG-REF was derived via a technology neutral aircraft scaling according to the project-specific TLARs. For REG-BAS and REG-CON, technology assumption factors for the year 2035+ were employed (see Table 2). The performance of the configurations was analyzed in an inner iteration loop of the mission, propeller and HEP system module. The mission module calculated the thrust demand for all mission points, which was then translated to a power demand by the propeller module. Here, the propeller was sized according to the mission requirements. The hybrid-electric power train, including the electrically assisted turboshaft, all electric components and the battery, was designed to meet the power demands in all mission points under the given constraints. To capture the effect of the unconventional HEP configuration on aircraft level, the behavior of the electrically assisted turboshaft was integrated via surrogate models. Masses of the propulsion-system-related components were added to the configuration and positioned by the positioning module. Convergence of the performance analysis was achieved through an MTOM convergence criterion.

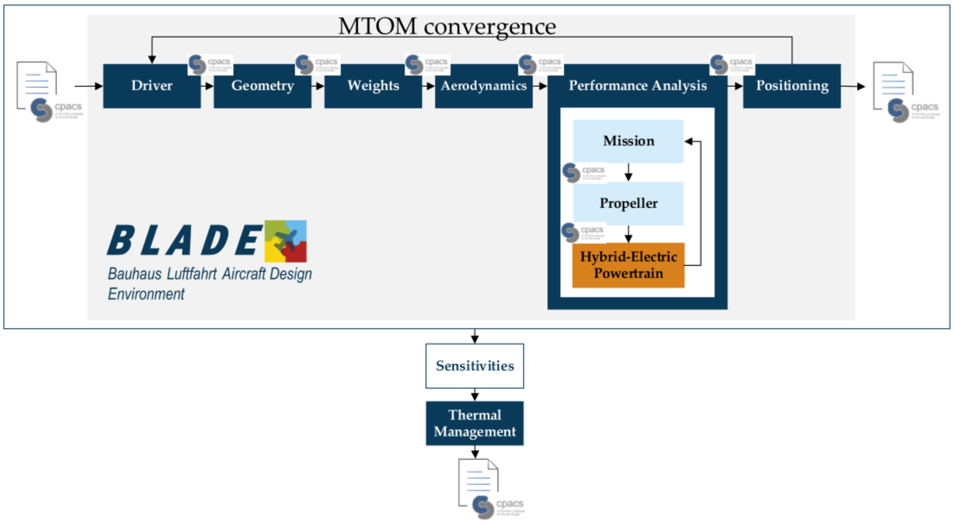

Figure 5. Aircraft design and sizing logic in BLADE.

To estimate the effect of the TMS on the aircraft performance for the REG-CON configuration, the TMS was considered in a post aircraft sizing step in the design and evaluation process.

3.2. Design Laws and Mission Definition

The target for the sizing of all reference and HEP aircraft was to minimize the typical mission block fuel. The design of the reference and HEP configurations followed several design rules.

The most important sizing laws for the baseline aircraft configurations were:

- Wing reference area (through wing loading)—LFL, TOFL and TODA at hot-day take-off with constant aspect ratio and wing span limitation according to ICAO Annex 14, Aerodrome Reference Code C [29];
- Wing planform—constant sweep, taper ratio and airfoils;
- Wing position—constant static stability margin (15%);
- Stabilizer and fin area—constant volume coefficients;
- Turboshaft engine—sized for hot-and-high take-off (ISA+30);
- Propeller diameter—constant propeller tip speed with blade pitch variation.

For the REG-CON, the following strategy was used for the sizing and analysis of the HEP system: all components were sized for a typical mission with the optimization goal of minimizing the typical mission block fuel. Independent parameters for the sizing of the hybrid-electric power train were the design power split $S_{p,des}$, the design hybridization degree $H_{p,des}$ and design shaft power $P_{shaft,des}$. Furthermore, the PLA (Power Lever Angle) served as an independent parameter for all off-design conditions.

The turboshaft engine was sized for TOC conditions with a prescribed $S_{p,des}$ and $H_{p,des}$. The electric components were sized according to the highest power requirement occurring during a typical mission. The battery was sized to meet the electrical energy demand along a typical mission, including the energy required for non-propulsive subsystems and the energy required for propulsion assistance.

For all other missions (design, hot-and-high take-off, payload-range), it was assumed that the same battery energy was available per flight segment compared to the typical mission results. The available battery energy was then spread over the mission segment so that the CIPH system (M-B) always required the same absolute power compared to the same segment of the typical mission, the energy required for the non-propulsive subsystems was subtracted from the battery energy and the remaining energy was supplied to the MIPH system (M-A). In cases in which the energy required for the non-propulsive subsystems exceeded the segment energy calculated for a typical mission (e.g., cruise for design mission with H_p = 0), the electric machine A (M-A) was used to generate the missing electrical power. As a result of this energy management strategy, H_p and S_p differed for the same segments of the different missions.

For all missions, it was assumed that the propulsion system was powered fully electrically during taxi-out and taxi-in. Furthermore, energy recuperation via the electric machine B (M-B) was used in descent to charge the battery using the electrical energy required for taxi-in. During this phase, it was ensured that the cycle-integrated motor did not feed power into the combustion engine and, thus, no electrical energy was used while charging. A constant charging power over the entire descent was assumed.

The sizing and point performance evaluation was based on the missions specified by the TLARs (Table 1). A design mission of 600 nmi was considered, while fuel burn was optimized for a typical 200 nmi mission. An additional typical mission with a 300 nmi range was considered to ensure the hot-day take-off TOFL requirement (see Table 1). LFL was evaluated for MLM, which was calculated as MTOM—300 kg for all aircraft. For all designs and typical missions, additional OEI (One Engine Inoperative) cases were considered. The REG-REFX turboshaft engine design point is TOC at Ma_{cruise} 0.46, FL220, ISA + 10 K. For all other reference aircraft, the design point is TOC at Ma_{cruise} 0.40, FL150, ISA + 10 K.

International reserves including 30 min holding at 1500 ft, 100 nmi alternate at 15,000 ft and 5% contingency fuel were taken into account as specified in the TLARs and in accordance with EC regulations, ICAO Annex 6 [30].

3.3. Systems Design and Integration

All disciplines and components relevant to the reference and HEP aircraft are described in the following section.

3.3.1. Aerodynamics

For a given aircraft geometry and specified flight conditions, a range of drag polars was calculated for low-speed and high-speed conditions using the aerodynamics module. The aerodynamic polars were saved in the CPACS data exchange file, and the performance analysis module extracted the relevant aerodynamic performance characteristics for all flight points of the calculated missions by interpolating between the polars. Lift, profile drag, induced drag and wave drag of all components were calculated by use of handbook methods provided by Torenbeek [27] and Raymer [28] with adaptions by Traub [31,32] and Lammering et al. [33]. Low-speed characteristics of the wing were calibrated to achieve a reference landing speed of 108 KCAS for the REG-REFX with MTOM and flaps 35° down in landing [34], thus achieving a landing C_{Lmax} of 2.67.

The profile drag calculation of the fuselage was adapted to account for the added belly fairing profile drag caused by the additional volume of the batteries inside the fuselage belly fairing.

3.3.2. Weights

The masses of the structural components were calculated with LTH (Luftfahrttechnisches Handbuch) handbook methods [35], which were calibrated to the OEM-scaled structural masses provided for an ATR aircraft by Obert [36].

Design payload was calculated using design capacity and passenger weights specified by the project TLARs. Most furnishing, operator and operational equipment masses provided by Obert were assumed to be unchanged for the REG-REF aircraft and were multiplied by the technology factor 0.8 for the aircraft with EIS 2035+.

Similarly, the OEM-scaled masses for the non-propulsive subsystems provided by Obert [36] were used for the REG-REF.

For REG-BAS and REG-CON, All-Electric Architectures (AEA) for the subsystems were assumed. While the REG-BAS used classic power off-takes from the turboshaft engines to provide the subsystem power requirements, the subsystem power demands of the REG-CON were sourced from the on-board batteries, making this a Universally Electric Subsystem Architecture (UESA).

To calculate the masses of the subsystems, weight factors, which can be found in the literature, were employed [37].

The positioning of the battery bays inside the fuselage belly fairing required the modification of the semi-empirical methods used for the fuselage structural weight calculation based on the added belly fairing wetted area. To account for the added structural masses of the high-aspect ratio wing with AR > 12, the semi-empirical LTH method MA 501 12 01 was modified based on wing structural weight simulation results presented in [38].

The estimation of the component masses related to the propulsion system as well as the battery are provided in Section 3.3.7.

3.3.3. Electrically Assisted Turboshaft

For calibration and the derivation of the REG-REF aircraft, a simplified turboshaft model was employed, which was derived and scaled to the PW127M design point from data on the PW120 engine presented by [39–41]. It was assumed that all power off-takes required for powering the non-propulsive subsystems were included in the engine data.

For propulsion system design and performance synthesis of the electrically assisted turboshaft engine, the framework Aircraft Propulsion System Simulation (APSS) was used.

First, a propulsion system model of the REG-BAS and REG-CON turboshaft engine (Figure 4) was set up in APSS. Initial propulsion system sizing was performed based on the aircraft results, shaft power requirements for the flight conditions as well as the initial hybridization assumptions from the IMOTHEP conceptual aircraft design Loop 0. Further details on the thermodynamic models and the propulsion systems assumptions can be found in [17].

The sizing demand and required performance characteristics of the propulsion system depend on the actual aircraft requirements in the aircraft conceptual design process. Thus, a parametric turboshaft model taking into account the different shaft power and hybridization requirements was created for overall aircraft integration. Advanced surrogate modeling techniques were employed to account for the increased turboshaft model complexity and the higher number of model parameters—such as $H_{p,des}$, $S_{p,des}$ or off-design H_p. In addition, a distinctive interface between the hybrid-electric power train modeling environment and the turboshaft surrogate model was implemented in order to avoid modeling errors and improve overall work flow performance.

Thus, surrogate models in the form of Feedforward Neural Networks (FNN) were derived and integrated in the aircraft design and sizing framework. The design and off-design characteristics of the electrically assisted turboshaft were reproduced using FNN, and were trained and validated with Latin Hypercube Sampled (LHS) [42] data as described in [43].

The model complexity was alleviated by reducing its input size to the most important parameters, which fully describe the performance characteristics of the electrically assisted turboshaft engine excluding any electric components such as power electronics, electric machines and battery systems. In addition, the MIPH system was not directly included in the turboshaft surrogate model. It was considered on an overall propulsion HEP system level by adding its electric power to the output shaft power of the turboshaft engine. The CIPH system, however, directly affects the performance characteristics of the gas turbine cycle. Thus, its electric power served as an input to the surrogate model.

The chosen parameterization of the turboshaft surrogate model enables the adaption of the turboshaft design point to different shaft power requirements and flight conditions. The flow-path sizing of the gas turbine was performed at TOC conditions with turboshaft geometry and weight (including year 2035+ technology assumptions) provided as an output of the surrogate model. Furthermore, important turboshaft design cycle parameters such as the burner exit temperature T_4 and the Overall Pressure Ratio (OPR) could be adapted, as well as the H_p of the CIPH system. For all off-design mission points, the flight conditions (ISA, altitude, *Ma*), PLA and the off-design cycle hybridization were required as inputs to the model. All relevant output parameters such as fuel flow and Power-Specific Fuel Consumption (PSFC) resulted from the evaluation of the FNNs.

The same turboshaft surrogate model was used for the REG-BAS as well as the REG-CON. In case of the non-hybrid REG-BAS application, it was ensured that the design and off-design H_p were zero.

For the mass estimation of the turboshaft engine, a simple heuristic based on Sea Level Static (SLS) take-off shaft power from [44] was used. The mass of the gearbox was estimated using a semi-empirical method. The gearbox efficiency was assumed to be constant for all flight points. Furthermore, propeller operational efficiencies were derived by scaling an existing propeller map from [45] to the design conditions of the turboshaft engine, ensuring a mid-cruise efficiency of 85%. Propeller mass estimation is based on the Hamilton Standard 568F propeller [46] and scaled linearly with the take-off power (SLS).

3.3.4. Battery

For the REG-CON configuration, the battery has a significant impact on its fuel burn reduction potential.

Battery pack design and off-design analyses were conducted with BHL in-house methods, which imported real cell data for current prototypes of hybrid Li-Metal batteries provided by [18]. The discharge characteristics (I–V characteristics) of the relevant cells were imported as two-dimensional look-up tables from [23]. By introducing an internal efficiency, the cell model was calibrated to match the published specific energy-specific power relations in [23].

To account for additional weight due to casings, local thermal management, containment, etc., a gravimetric cell-to-pack ratio of 0.742 was assumed for a lightweight pack design with pouch cells [47].

The battery pack was assumed to operate between an SoC of 95% and 20%. The battery was sized for an end-of-life state of health of 90%. Furthermore, a constant discharging/charging efficiency of 95% was assumed for one cycle.

3.3.5. Thermal Management System

The identification of the TMS impact on aircraft fuel burn was conducted as a post-sizing step to the aircraft sizing. The final REG-CON configuration was used to derive aircraft level sensitivities for added relative fuel burn (δFB) resulting from increments of drag, OEM and power off-takes.

The TMS study was fourfold, including the following steps:

1. Assessment of the available heat rejection rate (Q) via the existing aircraft surfaces with simple models from [25].
2. Design and optimization of a TMS utilizing an R-HEX based on the methods presented in [24].
3. Design and optimization of a TMS utilizing a modified version of the S-HEX or Wing Surface Heat Exchanger (WISH) presented in [21].
4. Selection of the best TMS combination for the given application case.

Modifications to the heat rejection models presented in [25] and the S-HEX model in [21] included the addition of a simple propeller model to calculate the slip stream velocity and the addition of micro-channels on the hot side of the S-HEX and are explained in detail in [48]. Reference [48] also contains various sensitivity studies, e.g., the influence of the propeller thrust on the available Q in multiple operating points as well as the results of step 1. Step 1 revealed that the aircraft had a heat rejection potential via the existing surfaces in excess of the expected waste heat in most operating points, which was a prerequisite to proceed with step 3.

Since the TMS assessment was not part of the main aircraft design loop, preliminary thermal inputs of the electric system were required to calculate ranges for the relevant TMS parameters mass m_{TMS}, drag D_{TMS} and power off-take $P_{off\text{-}take}$. A wide range of Q was chosen to allow flexibility in the choice of H_p. The outlet temperature (T_{out}) of the electric components was selected in accordance with their maximum operating temperatures. Two temperature levels were established: one for the battery and one for all other electrical components. For each temperature level, steps 2 and 3 were conducted separately.

The fuel burn sensitivity used for the optimization target functions in steps 2 and 3 was initially deduced for the REG-REFX configuration. Detailed TMS results can be found in [48].

The sensitivity function employed for the final REG-CON configuration typical mission ramp fuel burn is:

$$\delta FB = \frac{3.6\%}{1000\ \text{kg}} m_{TMS} + \frac{5.9\%}{1000\ \text{N}} D_{TMS} + \frac{0.2\%}{10000\ \text{W}} P_{off\text{-}take}. \quad (3)$$

Heat load trajectories were provided for all final REG-CON missions, which served as an input to the TMS selection. For both concepts, R-HEX and S-HEX, system mass, added aircraft drag and additional power off-take were calculated and the effect on aircraft level fuel burn was estimated using the function above. Finally, the aircraft level impact of both concepts was compared and the system was selected which had the smallest deterioration effect on typical mission fuel burn.

3.3.6. Non-Propulsive Subsystems

For the REG-REFX and REG-REF, the required gas turbine power off-takes of the non-propulsive subsystems are included in the turboshaft model. For the REG-BAS and REG-CON, an AEA or UESA were considered, respectively. The subsystems of the REG-BAS are powered using power off-takes from the gas turbine, while the UESA is sourced from the on-board primary batteries. Power off-takes of up to 200 kW were defined for all flight phases. It was differentiated between normal and emergency conditions. The masses of the required subsystems were calculated as presented in Section 3.3.2.

3.3.7. Electric Machines and Power Electronics

The modeling of all other components that are part of the HEP system interacts with numerous aircraft systems. The characteristics of all electric components, electric machines, inverters, converters, as well as cables, are represented by constant characteristics (gravimetric power density and efficiency). For the electric machines as well as the power electronics, liquid cooling was assumed [49].

The battery system provides 800 V Direct Current (DC) output, which is converted into 540 V DC and feeds into the power distribution. The high-power cables linking the components of the propulsion system are 540 V DC lines. The comparably long cables from the KV (Kilo Volt) DC bus to the inverters within the engine nacelles have the largest cable mass impact on aircraft level, as they feed the battery power from the belly fairing/lower fuselage to the wing-mounted propulsors. Identical to the battery–converter connection, the inverters are directly coupled to the electric machines. The mass of all cables was increased by a factor of 1.5 to account for connectors, sheath, jacket and installation accessories [49].

As the KVDC bus is the central distribution unit of the electric power, the breakdown of calculation considerations was split in systems upstream and downstream of the KVDC bus (see also Figure 3). Upstream of the KVDC bus, the battery is directly coupled to the converter. Multiple battery packs are distributed in two battery bays within the enlarged belly fairing and then connected to the KVDC bus. Downstream of the KVDC bus, three main calculation schemes were followed: the feed to the electric machines A and B (efficiency chain A and B) as well as the feed to the non-propulsive subsystems. The total specific power of the electric machines considers the active and passive parts as well as the housing. It was selected according to the required motor size. This also applies to the sizing of the power electronics [49].

The non-propulsive subsystems influenced the design of the HEP system. The flight-segment-specific constant power off-take values were fed into the battery design. This was also considered within the optimization of the propulsion system and in non-hybridized phases of the flight such as descent and landing.

The design of the HEP system was performed within the HEP module of the BLADE environment in close interaction with the other modules (Figure 5).

Once the HEP module had completed an HEP system design, all relevant masses, SoC, provided power and maximum available power of each mission point as well as a variety of hybridization-relevant parameters were stored in the CPACS file. Additionally, the turboshaft engine design parameters were stored for succeeding calculations regarding off-design characteristics.

4. Reference Aircraft

All IMOTHEP reference aircraft, i.e., the SoA REG-REF and the advanced REG-BAS, adhere to the TLARs stated in Table 2. The main characteristics, mass breakdowns, performance and payload range characteristics of the reference aircraft are summarized in Tables 3, A1–A3 and in Figure 6.

Table 3. Main characteristics of the studied aircraft.

Parameter		**Unit**	**REG-REFX**	**REG-REF**	**REG-BAS**	**REG-CON**
OEM		kg	11,600	10,580	10,820	15,570
MTOM		kg	18,600	16,445	16,420	21,300
Design mission	Block fuel	kg	1774	1221	1002	1063
	Ramp fuel [1]	kg	2366	1644	1381	1503
Typical mission	**Block fuel**	kg	611	430	359	321
	Ramp fuel [1]	kg	1135	832	706	724

[1] Sum of block and reserve fuel.

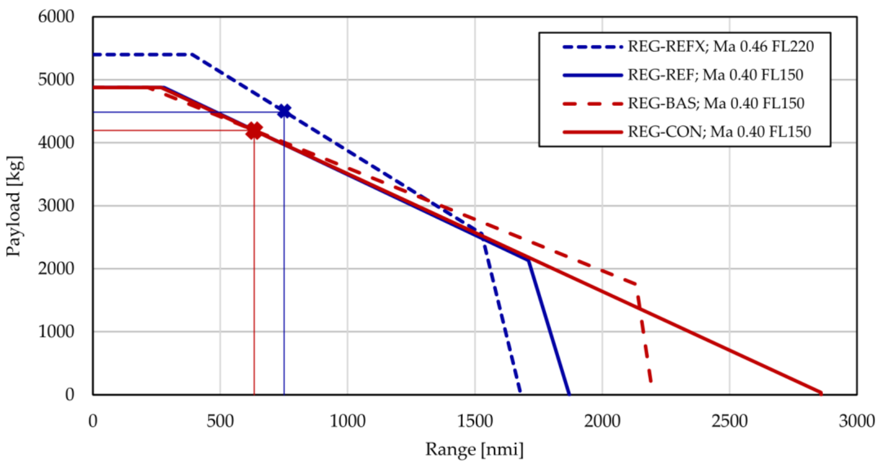

Figure 6. Payload-range characteristics of studied aircraft. Respective design missions indicated.

All conceptual aircraft design methods were calibrated to the REG-REFX.

Compared with the original ATR 42-600 (REG-REFX), the project-specific TLARs applied to the REG-REF are more relaxed (smaller design range and passenger capacity, lower design cruise speed and flight level) and, thus, a configuration with a significantly lower mission fuel burn resulted (see Table 3). The higher efficiency of the REG-REF compared with that of the REG-REFX can be mainly attributed to the reduction in cruise Mach (REG-REFX: Ma_{cruise} 0.46@FL220 vs. REG-REF: Ma_{cruise} 0.40@FL150).

The REG-BAS served as the main reference for comparing the effects of the proposed HEP concept against an evolutionary advanced conventional aircraft in 2035+. In addition to the TLARs applied to the REG-REFX and REG-REF, the REG-BAS and REG-CON faced a stricter TOFL requirement for hot-and-high take-off conditions. For the year 2035+, ISA+30 instead of ISA+20 conditions were assumed. Furthermore, the wing aspect ratio was increased to 14 and the non-propulsive subsystems advanced to an AEA architecture.

The combination of all effects resulted In an overall typical mission fuel burn reduction of 17% (see Table A1).

OEM and MTOM of the REG-BAS remain similar to the REG-REF and, thus, the wing area increased from 49 to 54 m^2 for the reduced wing loading (Table A1). OEM could not be reduced because the technological weight advancements postulated for the configuration were offset by the following component weight increases:

- The propulsion system mass was reduced only slightly, due to a higher TOC design thrust (see below), which partially offset the technological advances.
- Wing and vertical tailplane structural weights were increased because of the lifting surface area enlargement and a constant volume coefficient.
- Replacing the conventional non-propulsive subsystems with a UESA architecture led to a mass increase of 590 kg (Table A3).

Even though the increased wing aspect ratio caused a significant reduction in induced drag (~27% in mid-cruise conditions), the increase in VTP and wing area led to an increased aircraft profile drag (~7% at a 6% increased total aircraft surface area). In consequence, the aerodynamic efficiency *L/D* was improved by only ~3% in mid-cruise conditions (see Table A2).

The TOC design thrust of the turboshaft engine was also driven by the required take-off performance. Accordingly, TOC thrust was ~10% higher compared against the REG-REF. In accordance with the stipulated project target, the TSFC of the turboshaft engine in mid-cruise conditions was reduced by ~16% compared with that of the REG-REF (Table A2).

In summary, the aerodynamic efficiency was improved only slightly and the OEM was increased. Thus, the aircraft level fuel burn reduction stems mainly from the significant propulsion system performance improvements. These also led to the aircraft level efficiency improvements and ferry range increase depicted in the payload range diagram in Figure 6.

5. Hybrid-Electric Aircraft

To arrive at the final HEP aircraft results, pre-studies were conducted to investigate the behavior of the HEP architecture. Based on these, the final REG-CON was derived and compared against the REG-BAS. Trade studies were conducted, and the resulting sensitivities were used to estimate the effect of the TMS on fuel burn.

5.1. Non-Propulsive Subsystems

Apart from the propulsion system, the main difference between the REG-BAS and the REG-CON is the energy source of the non-propulsive subsystems. For the REG-CON, the subsystems are sourced directly from the battery instead of using power off-takes from the turboshaft. As the power required for the subsystems accounted for up to 200 kW in take-off, the battery energy required to source them along the whole mission was significant. Pre-studies showed that the battery weight attributed to the non-propulsive subsystems was more than 2 t if, in all missions (especially design mission) and all flight phases, the subsystems were fully powered by the battery. Thus, it was decided to only source the non-propulsive subsystem power in all flight phases of the typical mission from the battery (see figure in Section 5.3). For all other missions, the same energy per flight segment was used for sourcing the subsystems and all additionally required power was generated by the electric machine installed at the power shaft (M-A).

In summary, the architecture change of the non-propulsive subsystems alone led to a ramp fuel increase of 3.3% and a block fuel increase of 0.3% for a typical mission compared against the REG-BAS (e.g., Figure 7). This was mainly caused by the added battery weight of 1120 kg (ca. 6% MTOM) and subsequent cascade effects on aircraft level. The reserves part of the mission accounted for the biggest part of the ramp fuel increase because the aircraft performed especially worse in the holding segment compared with the REG-BAS.

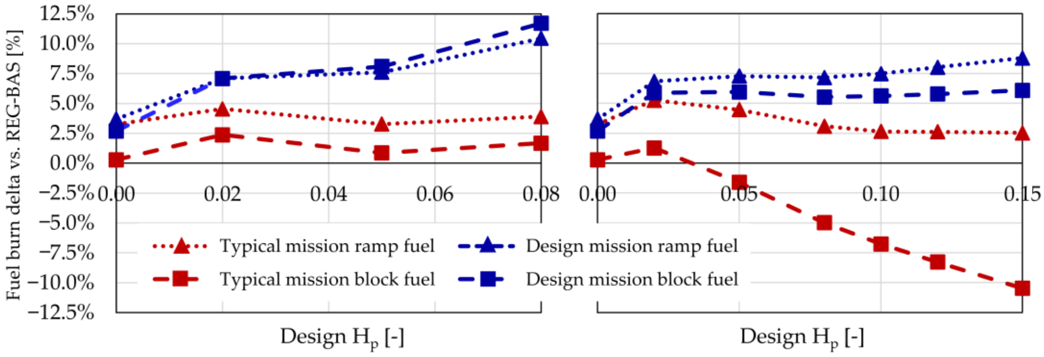

Figure 7. REG-CON mission fuel compared with REG-BAS for variation strategy 5 (**left**) and 6 (**right**).

5.2. Hybrid-Electric Powertrain System Behavior

At the aircraft level, the main objective of the project was to reduce typical mission fuel burn, similar to [7]. Pre-studies were conducted to refine the design space accordingly. The effect of the two most important parameters describing the HEP system, H_p and S_p, was investigated in a pre-study.

5.2.1. Operational Mission Hybridization Strategies

Choosing the most promising hybridization strategy is crucial to minimize typical mission block fuel. A hybridization strategy had to be found which ensured that the battery energy was optimally exploited from an aircraft level perspective [7,14]. Hybridization strategies define in which segments of the mission and to what extend an electrical assistance to the propulsion system is employed.

In an initial study, it was assumed that each design and off-design H_p as well as design and off-design S_p were similar for all mission segments with hybridization. For all strategies, taxi-in and taxi-out were fully electric and powered by the battery, and descent was used to generate enough electricity to electrically source taxi-in.

Different hybridization strategies were investigated. High-power strategies use electricity only in those flight phases that have the highest absolute propulsion power demand. This was intended to test if a smaller-sized turboshaft could suffice. Three high-power strategies were evaluated (strategies 1–3 in Table 4).

Aircraft level results of strategies 1–4 are depicted in Figure A1. All high-power strategies led to an increased mission fuel compared with that of the REG-BAS configuration due to the same effects. The weight of the additional electric components (electric motors, cables, converters and inverters) caused an immediate increase in aircraft weight compared with that of the REG-BAS, even for low H_p. Thus, a smaller *L/D* caused by a higher drag for higher H_p in almost all flight phases resulted and higher thrusts were required to propel the aircraft in most flight phases. To be able to meet the power requirements in all flight conditions with H_p = 0.0, the engine needed to be sized for a higher TOC design shaft power, which again led to a higher aircraft weight. Thus, even though the electrical assistance caused a more efficient propulsion system (TSFC reduction), it was offset by an increased thrust requirement, which caused a mission fuel burn increase. For cases with a mild hybridization ($H_{p,des} \leq 0.05$), the energy required from the battery to electrically assist the propulsion system was only small compared with the energy required to source the non-propulsive subsystems. For example, for strategy 3 and an $H_{p,des}$ = 0.05, the time-averaged battery power required for electrical assistance in take-off was 570 kW, while the battery power required for the non-propulsive subsystems was 225 kW. As electrical assistance was provided to the propulsion system only in a few short flight segments (e.g., strategy 3: take-off and go-around), the total battery energy required for propulsion only accounted for 3.4% of the total battery energy. The rest of the battery energy was used for the non-propulsive subsystems. Therefore, the added battery mass attributed to propulsion assistance was small in contrast to the weight added by the other additional electric components. The TOC design shaft power was increased and the wing loading could be decreased to meet the TLARs. Thus, the higher H_p, the smaller the wing area at an increased MTOM.

Table 4. Main hybridization strategies. Flight phases during which electrical assistance was employed are marked with "x".

Flight Phase/Strategy No.		1	2	3	4	5	6
Main mission	Taxi-out	x	x	x	x	x	x
	Take-off	x	x	x	x	x	x
	Climb	-	x	-	x	x	x
	Cruise	-	-	-	-	x	x
	Descent	Recuperation	Recuperation	Recuperation	Recuperation	Recuperation	Recuperation
Alternate and reserves	Go-around	-	-	x	x	x	-
	Diversion climb	-	-	-	x	x	-
	Diversion cruise	-	-	-	-	x	-
	Diversion descent	-	-	-	-	-	-
	Holding	-	-	-	-	x	-
	Holding descent	-	-	-	-	-	-
Main mission	Landing	-	-	-	-	-	-
	Taxi-in	x	x	x	x	x	x
Reserves	Contingency	-	-	-	-	x	-

All high-power strategies led to increased mission fuel burn, which was in the same range for typical and design missions when compared to the aircraft with $H_{p,des}$ = 0.0 and UESA of the non-propulsive subsystems. However, strategy 2 (take-off and climb of the main mission with electrical assistance) showed the most promising result (Figure A1, top right). For H_p = 0.035, typical mission block fuel was increased by less than 2% compared with the REG-BAS. Here, the turboshaft could be sized smaller, as it was allowed to use electrical assistance in the most critical flight phases of the typical mission, take-off as well as climb.

Strategy 4 can be interpreted as an extension of strategy 2 to the high-power segments of the reserves part of the mission. As depicted in Figure A1 (bottom right), no fuel burn reduction was achieved compared to the REG-BAS or the configuration with $H_{p,des}$ = 0.0, neither for the typical nor the design mission.

The results indicate that it is most beneficial to make use of the electrical assistance in the main mission cruise phase, which contributed the most to total block fuel, even for a regional aircraft with short mission ranges (ca. 45% for the typical mission and ca. 80% for the design mission).

Using electrical propulsion assistance in all flight phases of the mission resulted in the full hybridization or high-energy strategy 5. Mission fuel burn results for this strategy are depicted in Figure 7 (left). Both mission phases, main mission and reserves, contributed equally to the increase in fuel burn. Thus, block fuel and ramp fuel followed a similar trend for the typical and design mission.

For strategy 5, OEM and MTOM increased with $H_{p,des}$, as more electrical energy was required for the whole mission. Thus, battery weight increased and led to mass increase cascade effects on aircraft level. In addition, higher design shaft powers were required to meet all constraints. In combination, thrust demand was increased in all mission segments. For mild hybridization degrees ($H_{p,des} \leq 0.05$), the improved TSFC along the whole mission due to the electrical assistance offset, the higher thrust demands. However, for higher

$H_{p,des} > 0.05$, the turboshaft performance for some flight conditions (e.g., diversion descent) was worsened, which led to an overall fuel burn increase even for the typical mission.

The strategy with the highest typical mission block fuel burn reduction potential was strategy 6. Here, the introduction of the electric components required for electrical assistance of the propulsion system led to an increase in fuel burn for small $H_{p,des}$ (see Figure 7, right). A reduction in typical mission block fuel was observed for $H_{p,des} > 0.035$, which increased with increasing $H_{p,des}$. For configurations with $H_{p,des} > 0.15$, no configurations were found which met all aircraft level constraints.

However, typical mission ramp fuel decreased with increasing $H_{p,des}$, but was not reduced compared to the REG-BAS configuration. For the segments, which used electrical assistance, the propulsion system efficiency was improved (lower TSFC at higher thrust requirement) and fuel flow was reduced, even though the aircraft mass was increased due to the addition of the electric components and the added battery weight. For all reserve mission segments (diversion, holding and contingency), the aircraft mass was increased compared with the REG-BAS because of the added battery weight, which was required to electrically assist the main mission segments (e.g., +8.5% instantaneous aircraft weight at the beginning of holding for $H_{p,des} = 0.05$). Consequently, a higher thrust was required, but the propulsion system operated at a less efficient operating point with a higher TSFC. In summary, the increase in additional fuel required for the reserve mission segments offset the decreased fuel burn during the main mission, and ramp fuel was increased for the typical mission.

For the design mission, the increased thrust requirement offset the improved propulsion efficiency even for the main mission segment. Thus, design block fuel as well as design ramp fuel was increased compared with the REG-BAS.

In addition, the required source energy was explored for strategy 6. Results with respect to supply energy are visualized in Figure 8. Total block energy included block fuel energy and the total battery energy. With increasing $H_{p,des}$, the electrical energy stored in the battery increased linearly. At the same time, block fuel energy decreased proportionally with fuel weight, as observed before. The electrical energy required for the non-propulsive subsystems alone caused an increase in total block source energy by 9% compared with the REG-BAS. Fuel burn reduction with the addition of electrical energy, i.e., increase in $H_{p,des}$, could not offset the effect. Even though fuel burn was reduced with hybridization, total required source energy was increased. Thus, an ecological benefit could only result from charging the battery using fully sustainable energy sources.

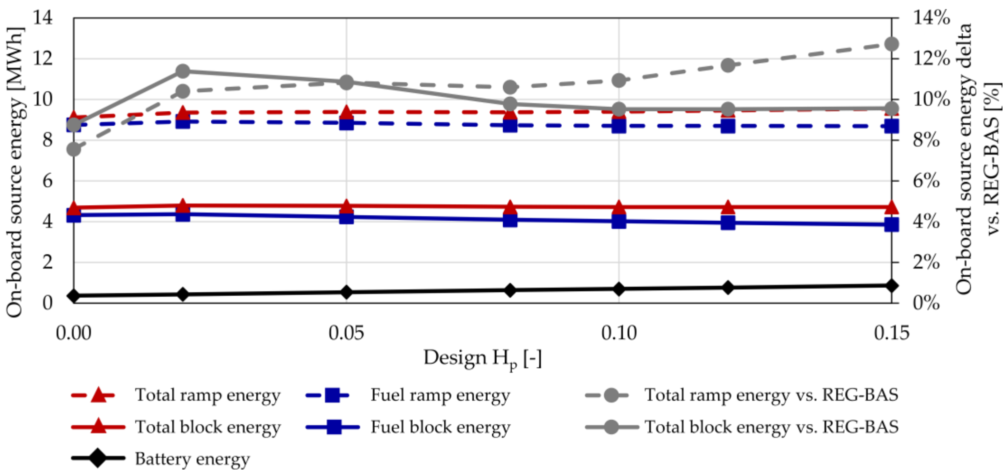

Figure 8. Typical mission source energy of REG-CON configurations of strategy 6. Division of battery and fuel source energy, total energy in absolute numbers and w.r.t. REG-BAS.

Based on the results of the hybridization strategy studies, the final REG-CON configuration was derived from strategy 6.

5.2.2. Power Split Optimization

Electrical cycle assistance can help to shift the operational point of the gas turbine, lead to higher gas turbine efficiency and, thus, increase the operational flexibility of the gas turbine. At $S_p = 0$, all electrical energy is used for cycle assistance; at $S_p = 1$, all electrical energy is employed for mechanical assistance of the power shaft.

In an initial study, $S_{p,des}$ was varied, while all other sizing parameters (e.g., wing loading, $H_{p,des}$) and the hybridization strategy were kept constant. In addition, the design power split was applied to all other off-design flight conditions with electrical assistance ($S_{p,des} = S_{p,off\text{-}des}$).

It was shown that for similar configurations with the same propulsion system design power, typical mission block fuel was reduced for higher S_p. Furthermore, the higher H_p, the bigger the fuel burn impact of S_p variation. The reason for this effect (reduced fuel burn for increased S_p) was mainly rooted in the efficiency of translating the available source energy into propulsive energy. Firstly, the efficiencies of the electric components varied for the electrical components of efficiency chain A and B. The tower shaft introduced additional losses within chain B. In consequence, the overall efficiency of chain A was higher compared with chain B. However, the propulsion architecture itself had an even bigger effect: together with the fuel energy supply, the electrical energy used to assist the turboshaft core (M-B) was routed through the power turbine and shaft system before arriving at the propeller power gearbox, to which M-A was directly connected. Thereby, the losses occurring in the power turbine and shaft system proportionately impacted the efficacy of the CIPH electrical assistance. Under the assumption of a constant design propulsion power and $H_{p,des}$, the gas turbine sizing power and, thus, the weight, reduced as S_p increased, while the combined weight of M-A and M-B was almost invariant. Cascade effects on aircraft level led to a decreased weight and subsequent reduction in required thrust.

In consequence, for most results presented for the hybridization strategy exploration, including the final REG-CON configuration, a minimum block fuel burn was achieved with maximum design and off-design power splits, i.e., all electrical energy was transferred to the motor installed at the power shaft.

To explore the effect of optimizing S_p in off-design conditions ($S_{p,des} \neq S_{p,off\text{-}des}$), the following design strategy was employed: for the design of the electrically assisted turboshaft in TOC conditions, $H_{p,des}$ and $S_{p,des}$ were prescribed. In addition, the same H_p was kept for all off-design flight conditions with hybridization. Within the aircraft design loop, the off-design S_p was then optimized individually for each point of each flight segment with an $H_p > 0$ with the goal of minimizing the instantaneous fuel flow. The result of such an optimization for a case with design and off-design $H_p = 0.02$, $S_{p,des} = 0.70$ and hybridization strategy 5 is depicted in Figure 9. The required power trajectories for both cases were similar due to the similar instantaneous gross weights.

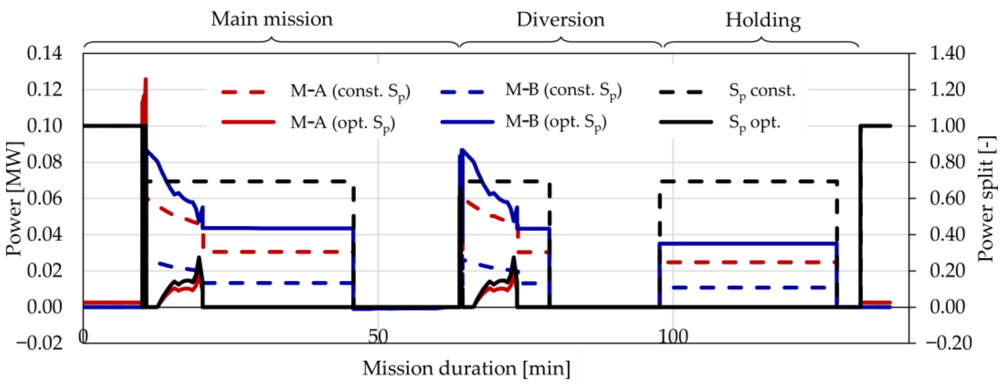

Figure 9. Power split, MIPH (M-A) and CIPH (M-B) power for typical mission of exemplary strategy 5 case with $H_p = 0.02$ and wing loading 300 kg/m^2, with constant $S_p = 0.70$ and with S_p optimization.

Figure 9 shows the (optimized) operational split of electrical power between M-A and M-B along a typical mission. In all taxi phases, S_p was unity and the propeller was driven by mechanical assistance through motor A. Even though the design power split was 0.70, the optimized operational power split stayed mostly below the design power split. With decreasing power requirements in both climb phases, S_p increased, but was reduced to 0 during cruise flight of the main mission as well as alternate and holding.

Compared to the same case, but with a constant $S_{p,des}$ = $S_{p,off\text{-}des}$, fuel burn could not be reduced significantly for those hybridization strategies, which did not require electrical energy in all segments of the mission. This was caused by the following effect: S_p was optimal in some segments for higher and in some segments for lower values compared with the design S_p. Thus, both electric motors had to be designed for higher critical power loads compared with the non-optimized case. As shown in Figure 9, for the case with constant S_p, the critical motor powers were ca. 80 kW (M-A) and 35 kW (M-B). For the optimized case, they amounted to ca. 125 kW and 90 kW, respectively. Thus, the weights of all electrical components were increased and, caused by cascade effects on aircraft level, MTOM was slightly increased. In consequence, fuel flow could be reduced in the segments with $H_p > 0$ due to the S_p optimization, but was slightly increased in all segments with $H_p = 0$ due to the increased power demand caused by the MTOM increase. In summary, optimizing the power split along the mission did not lead to a significant mission fuel burn decrease, but did not degrade it at the same time. Combining MIPH and CIPH could, thus, increase the operational flexibility of the turboshaft. For example, it should be investigated in detail if employing the CIPH in relevant flight conditions (e.g., high altitudes in cruise flight) leads to a local NOx emission reduction by operating the turboshaft at lower T_4 when it is supported by electric cycle assistance.

5.3. Aircraft Results

The final REG-CON configuration was chosen to be the configuration with the lowest typical mission block fuel compared with the REG-BAS. It featured an $H_{p,des}$ = 0.15 for the main mission take-off, climb and cruise phase (strategy 6). This can be translated to a ratio of total electrical power assistance to the engine shaft power of 30%. It achieved a typical mission block fuel reduction of 10.5% compared with the REG-BAS, while typical mission ramp fuel increased by 2.5% and design mission block fuel and ramp fuel increased by 6.1 and 8.8%, respectively.

The REG-CON's main specifications and performance characteristics are provided in the following subsections. In a post-processing step, it was estimated how the addition of the TMS affected the fuel burn performance of the configuration (see Section 5.5).

A three-view of the final REG-CON configuration geometry is presented in Figure 10. The fuselage is similar to that of the REG-BAS. Landing gear and extended belly fairing are not represented in the figure, but were accounted for in the calculations.

Its main characteristics are summarized and compared against the REG-BAS in Table A1. The wing area was increased by almost 30% compared with that of the REG-BAS due to the increased MTOM.

A mass breakdown of the REG-CON MTOM and comparison with the REG-BAS is provided in Table A3 and visualized in relative numbers in Figure 11. The battery mass accounted for 13% of MTOM. Lifting surface masses were impacted significantly by the increased wing area. The fuselage weight increased by only 1% due to the increased MTOM and added batteries. Electric motors, power electronics and cables accounted for ca. 35% of the propulsion system total weight. The DC-DC converters alone accounted for 2% MTOM.

The payload range diagrams for REG-REF, REG-BAS and REG-CON are depicted in Figure 6.

The maximum available fuel was significantly increased because of the increased wing area and volume. In addition, less fuel was required due to the electrical assistance. Thus, the maximum available fuel was higher than the assumed maximum structural payload, and the payload for maximum fuel was zero. In addition, the ferry range was increased compared with that of both REG-REF and REG-BAS.

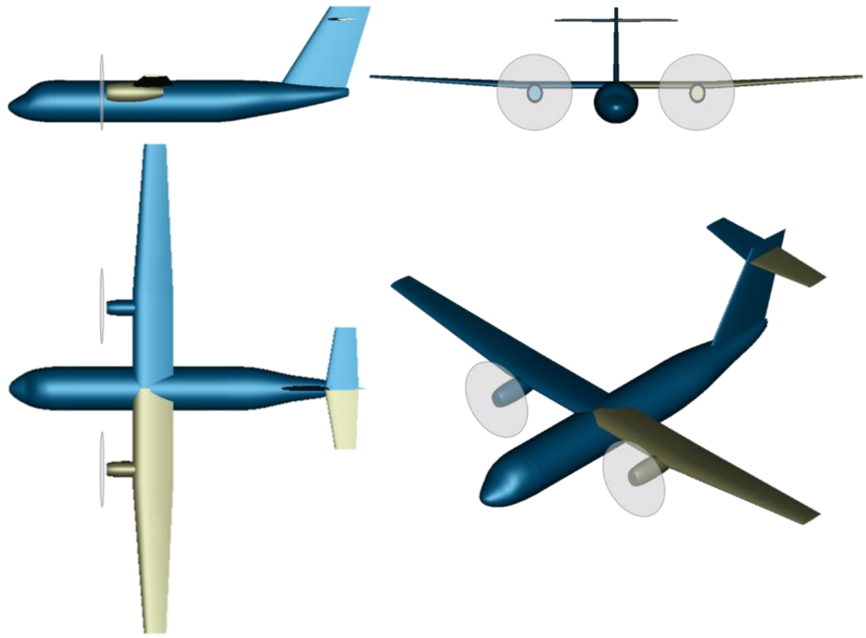

Figure 10. Three-view of REG-CON configuration.

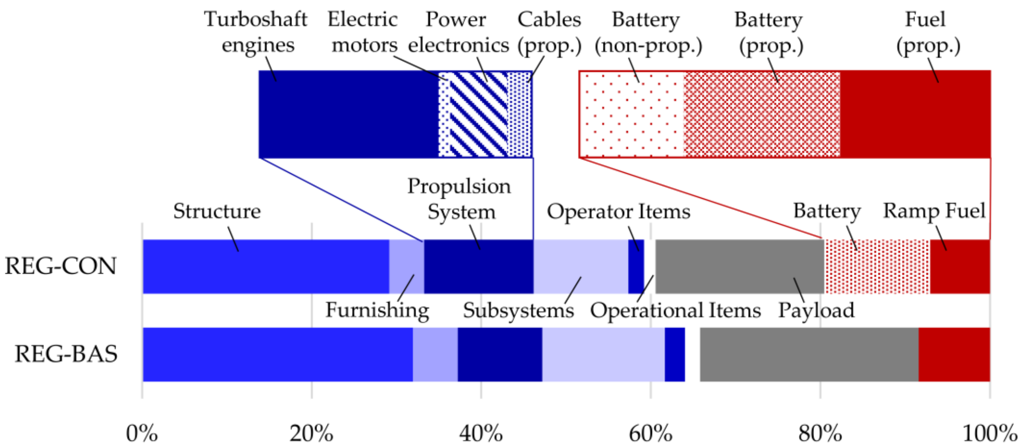

Figure 11. REG-BAS and REG-CON MTOM breakdown.

Exemplary propulsion system performance for characteristic flight conditions of the typical mission is provided in Table A2. Even though the required thrust in all flight conditions was increased, kerosene flow was reduced in these main mission flight conditions due to the highly improved turboshaft performance. For higher C_L, the aerodynamic performance of the aircraft was improved by an exemplary 6% in mid-cruise.

Figure 12 shows the power performance characteristics of the REG-CON along the typical mission. A maximum required turboshaft power of 6.7 MW was reached in take-off. This condition was critical for sizing the propulsion system, including all electrical components. The required battery power never exceeded 2.1 MW and remained close to 0.9 MW during cruise (Figure 12).

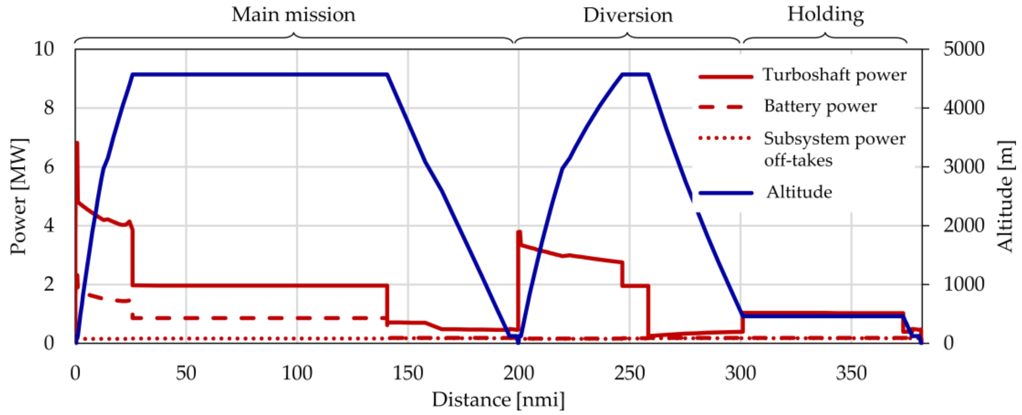

Figure 12. REG-CON typical mission required total turboshaft power, battery power, required non-propulsive subsystems power and altitude trajectory.

The performance characteristics of the battery and all electrical components of the HEP are summarized in Table 5. The battery's gravimetric energy at cell level was assumed to be 545 Wh/kg based on [19]. The corresponding gravimetric energy at pack level was 405 Wh/kg. The obtained instantaneous C-rates stayed below 2.5 C, with a mission-averaged C-rate of less than 0.5 C. Ca. 40% of the battery energy was required for sourcing the non-propulsive subsystems. The battery volume was <1 m^3 for each of the two battery bays.

Table 5. Performance characteristics of electrical components.

Component	Efficiency [%]	Gravimetric Energy Density [Wh/kg]	Gravimetric Power Density [kW/kg]	Gravimetric Density w.r.t. Length [kg/m]
Battery (pack)	95.0	400	-	-
Electric machines	97.6–98.7 [1]	-	11.3–17.1 [1]	-
DC-DC Converter	98.6 [1]	-	5.00 [1]	-
Inverters	99.1–99.4 [1]	-	11.2–16.8 [1]	-
Cables	99.6–99.7 [1]	-	-	3.00–4.50 [1]

[1] Source: [49].

5.4. Sensitivities

In order to gain a detailed understanding of the aircraft level behavior with respect to important design and technology parameters, one-dimensional sensitivity studies of the parameters defined in Table 6 were performed. The trade studies pivoted around the final REG-CON design described in Section 5.3.

All sensitivity studies emulated the influence of uncertainties in the technology advancement assumptions for the year 2035+, which were assumed for the REG-BAS and REG-CON aircraft. As presented in Table 6, component-level parameters were varied and a study of OEM weight factor and aircraft drag factor variation was conducted, which served as a proxy for a number of different parameters. The battery cell gravimetric energy density factor exploration covered a range of battery cell gravimetric energy densities from 300 to 1000 Wh/kg.

In the following, the focus was placed on the effect of the parameters on typical and design mission ramp fuel (incl. reserves). Across the sensitivity studies, all other design parameters were kept unchanged. Every point in the sensitivity studies represents a new aircraft design, including sizing effects.

Small variations around the REG-CON configuration values led to a linear response of typical and design mission ramp fuel for most of the studied parameters. Corresponding typical mission ramp fuel trade factors are presented Table 6. The trade factors for drag, OEM and power off-take variation were employed for the evaluation of the TMS.

Table 6. Trade study parameters and results.

Component	Study Parameters	Unit	Nominal	Limits	Behavior	Lin. Typ. Mission Fuel Burn Trade Factor δFB
Aircraft	OEM weight increment	kg	0.00	+/− 500 kg	Linear	+3.6%/+1000 kg
	Drag factor	-	1.00	0.95–1.05	Linear	+5.9%/+1000 N
Battery and electric components	Battery cell gravimetric energy density factor	-	1.00	0.55–1.80	Non-Linear	-
	Battery discharge/electric component efficiency increment	-	0.00	+/− 0.02	Linear	−0.1%/+1.0%
	Non-propulsive subsystem power off-take increment	kW	0.00	+/− 10.0 kW	Linear	+0.2%/+10 kW
Wing	Aspect ratio	-	14.0	12.0–14.0	Linear	+0.2%/−1.0 ΔAR

Uncertainties in the technological evolution of battery and electrical components until the year 2035+ were evaluated using a variation of battery discharge efficiency and battery cell gravimetric energy density with respect to the final REG-CON assumptions summarized in Table 6. Results are depicted in Figure 13. Improving the battery discharge efficiency by +/− 2% (η_{bat} = 97/93%) altered the efficiency of the electrical energy chain and, thus, more or less battery supply energy was required for the same hybridization strategy and mission. The aircraft level effect measured with typical and design mission ramp fuel was, however, only minor (−/+ 0.2% typical and design mission fuel, Figure 13 (left)) and could directly be attributed to the battery mass variation of −/+ 1.2%.

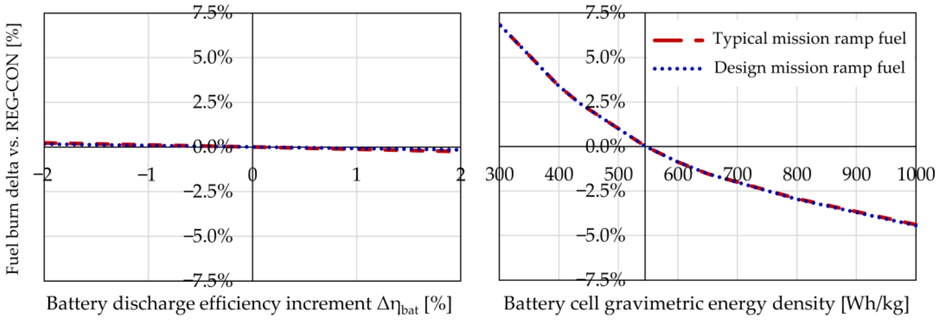

Figure 13. REG-CON fuel burn sensitivities on battery characteristics. Origin of the diagrams corresponds to the final REG-CON aircraft.

An improvement in the battery performance in terms of cell gravimetric energy can have a significant impact on the aircraft's performance, as visualized in Figure 13 (right). A cell level performance improvement of 20% (655 Wh/kg), corresponding to a similar battery mass reduction, led to an additional 1.5% ramp fuel decrease compared with the final REG-CON. The relationship between battery mass and mission fuel was approximated by a third order polynomial function. In total, 20% less optimistic battery assumptions (435 Wh/kg) corresponded to an even higher fuel burn increase of 2.4%.

5.5. Thermal Management System Effect

For the REG-CON configuration, the critical heat load, which sized the TMS, occurs in the typical mission take-off phase. Here, the time-averaged segment heat loads of the battery and all electrical components were bigger than those in all other flight segments and missions (>80 kW). It had been expected that the heat loads would be critical for hot-and-high take-off conditions. This, however, did not hold true for the presented sizing strategy of the HEP system. The HEP was sized for the typical mission with normal take-off conditions. For all other missions, it was assumed that each flight segment used the same amount of battery energy compared to the corresponding typical mission flight segment.

For these missions, including hot-day take-off, the duration of the take-off phase was longer compared with that of the typical mission, while the total take-off segment electrical energy was the same. Thus, the instantaneous battery power available during take-off was smaller. Correspondingly, the instantaneous battery heat loads of battery and electrical components were highest for the typical mission with the shortest take-off duration.

As described in Section 3.3.5, two different TMS scenarios were evaluated for each cooling circuit, i.e., the circuit for the battery as well as the combined circuit for all other electrical components.

In scenario 1, the entire heat load was rejected via an R-HEX. In scenario 2, an S-HEX was used, which was sized for the time-averaged cruise heat load. Any excessive heat which could not be rejected via the S-HEX was rejected by an added R-HEX. For this scenario, it was assumed that during cruise the R-HEX was not required. Thus, it could be turned off to not require any power, and the air inlet was considered to be closed to avoid any additional drag in cruise.

The results for both scenarios are summarized in Table 7.

Table 7. TMS scenario results for the REG-CON configuration. Chosen systems highlighted in bold.

Scenario	Component	TMS Mass [kg]	TMS Drag [N]	TMS Required Power [W]	Fuel Burn Increase Typical Mission [%]	Fuel Burn Increase Design Mission [%]
R-HEX	Battery	105	35	125	0.75	0.95
	Other electrical components	**20**	**5**	**20**	**0.13**	**0.17**
R-HEX + S-HEX	**Battery**	**1120**	**0**	**55**	**0.65**	**0.85**
	Other electrical components	25	0	30	0.14	0.18

The aircraft level sensitivity factors presented above were employed to estimate the effect of the added mass, drag and power on typical and design mission fuel. In order to minimize the fuel burn impact, two different scenarios were chosen for the different components. The battery made use of the above-described combination of R-HEX and S-HEX. All other electric components used the R-HEX as a heat sink for their entire heat loads.

In summary, the typical mission fuel burn was increased by 0.8% and design mission fuel burn was increased by 1.0% due to the added mass, drag and power demand of the TMS.

This led to an aircraft level fuel burn reduction potential of the REG-CON, including all effects of the TMS, of 9.6% compared with that of the REG-BAS for typical mission block fuel. Design mission block fuel increase amounted to 7.2% in total.

6. Discussion

As pointed out by Brelje and Martins, “It is widely known that specific energy of batteries [. . .] and specific power of electronics [. . .] strongly impact aircraft capabilities.” [4]. Analog to the results presented in literature (e.g., [2,10,14]) it was shown that the battery cell gravimetric energy density, i.e., the battery weight, has a significant impact on the fuel burn reduction potential of the aircraft configuration. However, for the study at hand, the impact of battery specific energy was found to be more significant than the specific power of the electrical components, because the battery weight accounts for a considerably bigger share of OEM compared with the propulsion-system-related electrical components.

Thus, the battery performance poses as the limiting factor for the near term market introduction of hybrid-electric aviation [3]. Significant battery performance improvements are required to increase the benefit of HEP on aircraft level. A roadmap for the evolution of battery performance within the next years was developed within the IMOTHEP project and is presented by Kühnelt et al. [19].

In consequence to the battery weight cascade effects on aircraft level, it was found that sourcing the non-propulsive subsystems directly from an on-board battery is not beneficial for the HEP aircraft architecture if the power required for the systems is as high as was assumed for this configuration. It could be promising to investigate a “more electric” subsystems architecture, wherein the electrical subsystems are sourced from generators attached to the power plants [37] or a strategic combination of generators and batteries is utilized [50].

Different hybridization strategies were studied. Results for the differing strategies vary significantly, and choosing the best strategy depends on the fuel burn reduction potential of the HEP configuration as indicated by [7,14]. It was found that pure high-power strategies as well as electrically assisting the propulsion system during the reserves phase of the mission is not beneficial to reduce mission fuel burn. Results indicated, however, that it is favorable to employ hybridization in the cruise phase, which is in line with the findings of Orefice et al. [7]. They argue that the time related to cruise is longer compared with take-off and climb and, thus, a higher energy-saving potential exists for the cruise phase [7]. The most promising hybridization strategy is to employ hybridization in main mission take-off, climb and cruise. Further investigations shall study the additional potential of more refined hybridization strategies.

Splitting the available electric power between MIPH and CIPH does not have a significant effect on aircraft level. For most evaluated configurations, a pure mechanical assistance achieves a slightly higher fuel burn reduction. However, the objective of the aircraft design process was to minimize fuel burn. It did not resolve NO_x emissions along the mission trajectory. Employing the CIPH assistance in relevant flight conditions (e.g., high altitudes in cruise flight) promises a local NO_x emission reduction by operating the turboshaft at lower T_4 when it is supported by electric cycle assistance. Thus, the added CIPH assistance can potentially increase the operational flexibility of the turboshaft and lead to a reduction in non-CO_2 climate effects at a small fuel burn expense. This effect has to be studied in detail in the future.

Combining a conventional R-HEX and an innovative S-HEX TMS shows a synergistic effect with the investigated HEP turboprop configuration. A combination of both systems allows for a smaller aircraft performance degradation compared with a purely conventional (R-HEX) system.

Additional technologies, such as distributed propulsion, wingtip propulsion and blown wings, promise synergistic effects when combined with an HEP architecture [12]. The added fuel burn reduction potential of the presented configuration in combination with these technologies will have to be investigated in the future.

To estimate the emission reduction potential of this aircraft configuration in contrast to fuel burn, a well-to-wake analysis has to be conducted. Furthermore, the economic feasibility of the configuration will have to be evaluated to determine the probability for an entry into market in 2035+. The economic analysis might be based on the method presented by Antcliff et al. [11].

7. Conclusions

Comprehensive aircraft level studies were conducted for a regional HEP aircraft with twofold electrical assistance and EIS 2035+. Its results aimed at narrowing down the uncertainties when estimating the potential of regional HEP configurations and to serve as a reference for the HEP roadmap developed within the IMOTHEP project.

The investigated configuration features an HEP architecture with a twin-engine propulsion system using twofold electrical assistance to the turboshaft. A combination of kerosene (stored in wing tanks) and hybrid Li-Metal batteries (stored in front of and behind the main body landing gear inside an extended belly fairing) serve as on-board energy sources for the propulsion system. Furthermore, hybrid Li-Metal batteries were employed as the sole energy source for UESA. The electrically assisted turboshaft features a three-spool architecture. A CIPH system provides electrical assistance to the high-pressure spool via a tower shaft. An additional MIPH system is located on the power shaft behind the propeller gearbox. To exploit synergistic effects of the required TMS with the aircraft architecture, a conventional R-HEX and an innovative S-HEX are combined.

Results indicated that the main limiting technological factor for exploiting the potential of the hybrid-electric aircraft concept is the gravimetric energy density of the battery. Choosing an optimal mission hybridization strategy is key to achieving a maximum fuel burn reduction for a given configuration from an operational perspective. It can be concluded that it is beneficial to employ electrical assistance during the longer phases of the main mission (e.g., cruise). Electrical energy should not be used for propulsion during the diversion and holding phase. Additionally, it is unfavorable to source the non-propulsive subsystems directly from the on-board battery.

Based on the study results, the final hybrid-electric REG-CON configuration was derived with a hybridization degree of H_p = 0.15 in all hybrid mission segments. It achieved a typical mission block fuel reduction of 10.6%. However, typical mission ramp fuel as well as design mission block and ramp fuel increased. Including the effects of the TMS on aircraft level performance in a post-processing step reduced the typical mission block fuel reduction potential to 9.6% compared with that of the conventional reference aircraft REG-BAS.

Author Contributions: Conceptualization, A.L.H., F.P. and A.S.; methodology, A.L.H., H.K., M.G.K., P.M., C.R. and A.S.; software, A.L.H., H.K., M.G.K., P.M. and C.R.; validation, A.L.H.; formal analysis, A.L.H., H.K., M.G.K., P.M. and C.R.; investigation, A.L.H., H.K., M.G.K., P.M., C.R. and A.S.; writing—original draft preparation, A.L.H., H.K., M.G.K., P.M. and C.R.; writing—review and editing, A.L.H., H.K., M.G.K., P.M., F.P., C.R. and A.S.; visualization, A.L.H., P.M., C.R. and A.S.; supervision, F.P. and A.S.; project administration, A.S.; funding acquisition, A.S. All authors have read and agreed to the published version of the manuscript.

Funding: This research was funded by the European Union's Horizon 2020 research and innovation program under grant agreement No. 875006.

Institutional Review Board Statement: Not applicable.

Informed Consent Statement: Not applicable.

Data Availability Statement: Not applicable.

Acknowledgments: The authors would like to thank the Visionary Aircraft Concepts team at Bauhaus Luftfahrt e.V. for their continuous support and development of the aircraft design environment BLADE. We especially thank Michael Shamiyeh for his contribution and integration of the battery module. We would also like to show our gratitude to our colleagues from Leonardo Aircraft for providing the project-specific TLARs, supporting the derivation of the year 2035+ technology assumptions and validating the reference aircraft.

Conflicts of Interest: The authors declare no conflict of interest. The funders had no role in the design of the study; in the collection, analyses or interpretation of data; in the writing of the manuscript; or in the decision to publish the results.

Abbreviations

The following abbreviations are used in this manuscript:

AEA	All-Electric Architectures
AEO	All-Engines Operative
APSS	Aircraft Propulsion System Simulation
AR	Aspect Ratio
ATR	Avions de Transport Régional
BAT	BATtery
BHL	Bauhaus Luftfahrt e.V.
BLADE	Bauhaus Luftfahrt Aircraft Design Environment
C	Cable
CIPH	Cycle-Integrated Parallel Hybrid
CoG	Center of Gravity

CONV	CONVerter
CPACS	Common Parametric Aircraft Configuration Schema
DC	Direct Current
EIS	Entry-Into-Service
EM	Empty Mass
FNN	Feedforward Neural Networks
FutPrInt50	Future Propulsion and Integration: towards a hybrid-electric 50-seat regional aircraft
GB	GearBox
GT	Gas Turbine
HECARRUS	Hybrid ElectriC smAll commuteR aiRcraft conceptUal deSign
HEP	Hybrid-Electric Propulsion
HPC	High-Pressure Compressor
HP	High-Pressure
IMOTHEP	Investigation and Maturation of Technologies for Hybrid-Electric Propulsion
INV	INVerter
IRON	Innovative turbopROp configuratioN
ISA	International Standard Atmosphere
KV	Kilo Volt
LFL	Landing Field Length
LHS	Latin Hypercube Sampled
LTH	Luftfahrttechnisches Handbuch
M	Motor
MIPH	Mechanically Integrated Parallel Hybrid
MLM	Maximum Landing Mass
MTOM	Maximum Take-Off Mass
OEI	One Engine Inoperative
OEM	Operational Empty Mass
OPR	Overall Pressure Ratio
PAX	Passengers
PEGASUS	Parallel Electric-Gas Architecture with Synergistic Utilization Scheme
PLA	Power Lever Angle
PMAD	Power Management And Distribution
PROP	PROPeller
PSFC	Power-Specific Fuel Consumption
REG-BAS	REGional-BASeline
REG-CON	REGional-CONservative
REG-REF	REGional-REFerence
R-HEX	Ram-air Heat EXchangers
S-HEX	Surface Heat EXchangers
SL	Sea Level
SLS	Sea Level Static
SoA	State-of-the-Art
SoC	State of Charge
SUB	SUBsystems
TOC	Top-Of-Climb
TODA	Take-Off Distance Available
TOFL	Take-Off Field Length
TLAR	Top-Level Aircraft Requirements
TMS	Thermal Management System
TOFL	Take-Off Field Length
TOM	Take-Off Mass
TS	Tower Shaft
TSFC	Thrust-Specific Fuel Consumption
UESA	Universally Electric Subsystem Architecture
WISH	Wing Surface Heat Exchanger

Appendix A

Table A1. Characteristics of the studied aircraft.

Parameter		Unit	REG-REFX	REG-REF	REG-BAS	REG-CON	REG-BAS vs. REG-REF [%]	REG-CON vs. REG-BAS [%]
OEM		kg	11,600	10,580	10,820	15,570	+2.3	+44
MTOM		kg	18,600	16,445	16,420	21,300	0.0	+30
Wing loading		kg/m^2	340	337	305	305	−10	0.0
Aspect ratio		-	11.0	11.0	14.0	14.0	+27	0.0
Wing area		m^2	54.5	48.8	53.8	69.8	+10	+30
Wing span		m	24.5	23.2	27.4	31.3	+18	+14
MAC		m	2.29	2.16	2.02	2.3	−6.5	+15
C_{Lmax} (landing)		-	2.67	2.71	2.71	2.71	0.0	0.0
Design mission	Payload	kg	4560	4240	4240	4240	-	-
	Range	nmi	716	600	600	600	-	-
	Block fuel	kg	1774	1221	1002	1063	−18	+6.1
	Reserve fuel	kg	592	442	379	440	−14	+16
	Ramp fuel	kg	2366	1644	1381	1503	−16	+8.8
Typical mission	Payload	kg	4560	4240	4240	4240	-	-
	Range	nmi	200	200	200	200	-	-
	Block fuel	**kg**	**611**	**430**	**359**	**321**	**−17**	**−11**
	Reserve fuel	kg	525	402	347	403	−14	+16
	Ramp fuel	kg	1135	832	706	724	−15	+2.5

Table A2. Performance in SLS take-off, TOC and mid-cruise of REG-REF, REG-BAS and REG-CON typical missions.

		REG-REF			REG-BAS			REG-CON		
		SLS	**TOC**	**Mid-Cruise**	**SLS**	**TOC**	**Mid-Cruise**	**SLS**	**TOC**	**Mid-Cruise**
Ma/FL/ISA	−/100 ft/K	0.0/0/0	0.40/150/10	0.40/150/0	0.0/0/0	0.40/150/10	0.40/150/0	0.0/0/0	0.40/150/10	0.40/150/0
Shaft power per engine	MW	1.9	1.0	0.8	1.9	1.1	0.8	2.8	1.9	1.0
TSFC	g/kN/s	5.5	12.6	12.6	3.6	9.6	10.5	2.6	6.3	6.9
L/D	-	-	14.2	14.2	-	14.5	14.6	-	15.4	15.4
Instantaneous weight	kg	15,620	15,450	15,350	15,750	15600	15,550	20,500	204,500	20,350

Table A3. MTOM breakdown of the studied aircraft. Values in kg.

Parameter	REG-REFX	REG-REF	REG-BAS	REG-CON	REG-BAS vs. REG-REF [%]	REG-CON vs. REG-BAS [%]
Payload	4560	4240	4240	4240	0.0	0.0
OEM	11,600	10,580	10,820	15,570	2.3	+44
EM	106,70	9730	10,140	14,890	4.2	+47
Structure	5880	5180	5250	6210	1.3	+18
Fuselage	2930	2790	2590	2630	−7.0	+1.2
Wing	1745	1420	1650	2180	17	+36
HTP	245	180	170	270	−5.0	+55
VTP	360	270	330	500	22	+50
Landing gear	595	530	500	650	−5.1	+30
Propulsion system (total)	1910	1660	1640	2760	−1.6	+69
Turboshaft engines (total)	1910	1660	1640	1800	−1.6	+10
Electric motors (total)	0	0	0	120	-	-
Power electronics (total)	0	0	0	580	-	-
Cables (total)	0	0	0	250	-	-
Furnishing	1090	1090	870	870	−20	0.0
Non-propulsive subsystems	1790	1790	2380	2380	33	0.0
Operator items	570	490	390	390	−20	-
Operational items	360	360	290	290	−20	-
Battery	0	0	0	2670	−17	-
Design ramp fuel	2440	1650	1370	1490	-	+8.8
MTOM	18,600	16,450	16,420	21,300	0.0	+30
MLM	18,300	16,150	16,120	21,000	0.0	+30

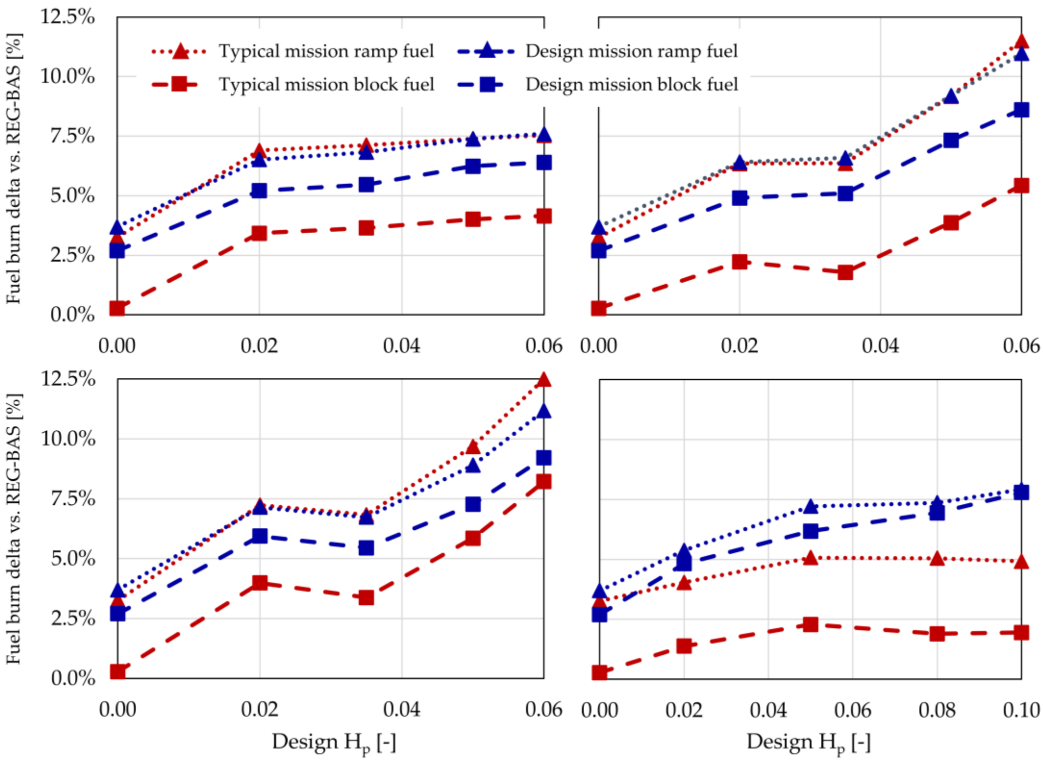

Figure A1. REG-CON mission fuel compared with REG-BAS reference for $H_{p,des}$ variation strategy; 1 (**top left**), 2 (**top right**), 3 (**bottom left**) and 4 (**bottom right**).

References

1. Isikveren, A.T.; Seitz, A.; Vratny, P.C.; Pornet, C.; Ploetner, K.O.; Hornung, M. Conceptual Studies of Universally-Electric Systems Architectures Suitable for Transport Aircraft. In *61. Deutscher Luft- und Raumfahrtkongress (DLRK)*; Deutsche Gesellschaft für Luft-und Raumfahrt, Ed.; DLRK: Berlin, Germany, 2012.
2. Pornet, C.; Isikveren, A.T. Conceptual design of hybrid-electric transport aircraft. *Prog. Aerosp. Sci.* **2015**, *79*, 114–135. [CrossRef]
3. Thomson, R.; Baum, M.; Kirschstein, T.; Martinez, N.; Sachdeva, N.; Lepine, P.-L.; Bailly, N. Aircraft Electrical Propulsion—Onwards and Upwards. In *Think:Act*; Roland Berger, Ed.: London, UK, 2018.
4. Brelje, B.J.; Martins, J.R. Electric, hybrid, and turboelectric fixed-wing aircraft: A review of concepts, models, and design approaches. *Prog. Aerosp. Sci.* **2019**, *104*, 1–19. [CrossRef]
5. Sahoo, S.; Zhao, X.; Kyprianidis, K. A Review of Concepts, Benefits, and Challenges for Future Electrical Propulsion-Based Aircraft. *Aerospace* **2020**, *7*, 44. [CrossRef]
6. Voskuijl, M.; van Bogaert, J.; Rao, A.G. Analysis and design of hybrid electric regional turboprop aircraft. *CEAS Aeronaut. J.* **2018**, *9*, 15–25. [CrossRef]
7. Orefice, F.; Nicolosi, F.; Corcione, S.; Della Vecchia, P. Hybridization and Mission Analysis of a regional turboprop. In *AIAA Aviation 2021 Forum, Virtual Event*; American Institute of Aeronautics and Astronautics: Reston, VA, USA, 2021; ISBN 978-1-62410-610-1.
8. Antcliff, K.R.; Capristan, F.M. Conceptual Design of the Parallel Electric-Gas Architecture with Synergistic Utilization Scheme (PEGASUS) Concept. In Proceedings of the 18th AIAA/ISSMO Multidisciplinary Analysis and Optimization Conference, Denver, CO, USA, 5–9 June 2017; American Institute of Aeronautics and Astronautics: Reston, VA, USA, 2017. ISBN 978-1-62410-507-4.
9. Nasoulis, C.P.; Gkoutzamanis, V.G.; Kalfas, A.I. Multidisciplinary conceptual design for a hybrid-electric commuter aircraft. *Aeronaut. J.* **2022**, *126*, 1242–1264. [CrossRef]
10. Moebs, N.; Eisenhut, D.; Windels, E.; van der Pols, J.; Strohmayer, A. Adaptive Initial Sizing Method and Safety Assessment for Hybrid-Electric Regional Aircraft. *Aerospace* **2022**, *9*, 150. [CrossRef]
11. Antcliff, K.R.; Guynn, M.D.; Marien, T.; Wells, D.P.; Schneider, S.J.; Tong, M.J. Mission Analysis and Aircraft Sizing of a Hybrid-Electric Regional Aircraft. In Proceedings of the 54th AIAA Aerospace Sciences Meeting 2016, San Diego, CA, USA, 4–8 January 2016; Curran Associates Inc.: Red Hook, NY, USA, 2016. ISBN 978-1-62410-393-3.
12. Thauvin, J.; Barraud, G.; Budinger, M.; Roboam, X.; Leray, D.; Sareni, B. Hybrid Regional Aircraft: A Comparative Review of New Potentials Enabled by Electric Power. In Proceedings of the 52nd AIAA/SAE/ASEE Joint Propulsion Conference, Salt Lake City, UT, USA, 25–27 July 2016; American Institute of Aeronautics and Astronautics: Reston, VA, USA, 2016. ISBN 978-1-62410-406-0.
13. Cameretti, M.; Del Pizzo, A.; Di Noia, L.; Ferrara, M.; Pascarella, C. Modeling and Investigation of a Turboprop Hybrid Electric Propulsion System. *Aerospace* **2018**, *5*, 123. [CrossRef]

14. Hoelzen, J.; Liu, Y.; Bensmann, B.; Winnefeld, C.; Elham, A.; Friedrichs, J.; Hanke-Rauschenbach, R. Conceptual Design of Operation Strategies for Hybrid Electric Aircraft. *Energies* **2018**, *11*, 217. [CrossRef]
15. Spierling, T.; Lents, C.E. Parallel Hybrid Propulsion System for a Regional Turboprop: Conceptual Design and Benefits Analysis. In Proceedings of the AIAA Propulsion and Energy 2019 Forum, Indianapolis, IN, USA, 19–22 August 2019; American Institute of Aeronautics and Astronautics: Reston, VA, USA, 2019. ISBN 978-1-62410-590-6.
16. IMOTHEP Consortium. Available online: imothep-project.eu (accessed on 10 November 2022).
17. Maas, P. Performance Investigations of a Cycle- and Mechanically-Integrated Parallel Hybrid-Electric Turboshaft. *Aerospace*, 2023; *to be published*.
18. Vratny, P.C.; Kaiser, S.; Seitz, A.; Donnerhack, S. Performance Investigation of Cycle-Integrated Parallel Hybrid Turboshafts. *J. Eng. Gas Turbines Power* **2017**, *139*, 031201. [CrossRef]
19. Kühnelt, H.; Mastropierro, F.; Zhang, N.; Toghyani, S.; Krewer, U. Are batteries fit for hybrid-electric regional aircraft? *J. Phys. Conf. Ser.* 2023; *in preparation*.
20. Seitz, A.; Nickl, M.; Stroh, A.; Vratny, P.C. Conceptual study of a mechanically integrated parallel hybrid electric turbofan. *Proc. Inst. Mech. Eng. Part G J. Aerosp. Eng.* **2018**, *232*, 2688–2712. [CrossRef]
21. Kellermann, H.; Habermann, A.L.; Vratny, P.C.; Hornung, M. Assessment of fuel as alternative heat sink for future aircraft. *Appl. Therm. Eng.* **2020**, *170*, 114985. [CrossRef]
22. Seitz, A.; Peter, F. Aircraft Concept for IMOTHEP Conservative Regional Platform Bauhaus Luftfahrt Presentation Delivered to ONERA. E-Mail. 2019.
23. Mikhaylik, Y.; Kovalev, I.; Scordillis-Kelly, C.; Liao, L.; Laramie, M.; Schoop, U.; Kelley, T. 650 Wh/kg, 1400 Wh/L Rechargeable Batteries for New Era of Electrified Mobility. In Proceedings of the 2018 NASA Aerospace Battery Workshop, Huntsville, AL, USA, 27–29 November 2018.
24. Kellermann, H.; Lüdemann, M.; Pohl, M.; Hornung, M. Design and Optimization of Ram Air–Based Thermal Management Systems for Hybrid-Electric Aircraft. *Aerospace* **2021**, *8*, 3. [CrossRef]
25. Kellermann, H.; Habermann, A.L.; Hornung, M. Assessment of Aircraft Surface Heat Exchanger Potential. *Aerospace* **2020**, *7*, 1. [CrossRef]
26. Deutsches Zentrum für Luft- und Raumfahrt. CPACS. Available online: cpacs.de (accessed on 30 May 2023).
27. Torenbeek, E. *Synthesis of Subsonic Airplane Design: An Introduction to the Preliminary Design of Subsonic General Aviation and Transport Aircraft, with Emphasis on Layout, Aerodynamic Design, Propulsion and Performance*; Springer: Dordrecht, The Netherlands, 1982; ISBN 9789048182732.
28. Raymer, D.P. *Aircraft Design: A Conceptual Approach*, 6th ed.; American Institute of Aeronautics and Astronautics Inc.: Reston, VA, USA, 2018; ISBN 978-1-62410-490-9.
29. International Civil Aviation Organization. Aerodromes: Volume I—Aerodrome Design and Operations Annex 14 to the Convention on International Civil Aviation. 2016. Available online: https://skylibrarys.files.wordpress.com/2016/07/annex-14-aerodromes.pdf (accessed on 30 May 2023).
30. International Civil Aviation Organization. Operation of Aircraft: Part I—International Commercial Air Transport—Aeroplanes Annex 6 to the Convention on International Civil Aviation. 2010. Available online: https://ffac.ch/wp-content/uploads/2020/09/ICAO-Annex-6-Operation-of-Aircraft-Part-I-International-commercial-air-transport.pdf (accessed on 30 May 2023).
31. Traub, L.W. Analytic Drag Prediction for Cambered Wings with Partial Leading Edge Suction. *J. Aircr.* **2009**, *46*, 312–319. [CrossRef]
32. Traub, L.W. Camber Effects on Minimum Power and Thrust Relations for Propeller Aircraft. *J. Aircr.* **2016**, *53*, 299–304. [CrossRef]
33. Lammering, T.; Eckhard, A.; Henke, R. Validation of a Method for Fast Estimation of Transonic Aircraft Polars and its Application in Preliminary Design. In Proceedings of the RAeS Aerodynamics Conference 2010: Applied Aerodynamics: Capabilities and Future Requirements, London, UK, 27–28 July 2010.
34. Avions de Transport Regional. Airplane Flight Manual: ATR 42 Models 400–500. 1995. Available online: https://www.google.com/url?sa=t&rct=j&q=&esrc=s&source=web&cd=&cad=rja&uact=8&ved=2ahUKEwiS0IHXg6H_AhWNHXAKHfbFDMMQFnoECBMQAQ&url=https%3A%2F%2Fwww.easa.europa.eu%2Fen%2Fdownloads%2F7358%2Fen&usg=AOvVaw0OdHaUiXl8-XJV07ReJe82 (accessed on 30 May 2023).
35. Arbeitskreis Masseanalyse (MA). *Luftfahrttechnisches Handbuch*; LTH-Koordinierungsstelle (IABG mbH): Ottobrunn, Germany, 2015.
36. Obert, E. *Aerodynamic Design of Transport Aircraft*; IOS Press: Amsterdam, The Netherlands, 2009; ISBN 9781586039707.
37. Chakraborty, I. Subsystem Architecture Sizing and Analysis for Aircraft Conceptual Design. Ph.D. Thesis, Georgia Institute of Technology, Atlanta, GA, USA, 2015.
38. Kling, U.; Empl, D.; Boegler, O.; Isikveren, A.T. Future Aircraft Wing Structures Using Renewable Materials. In *64. Deutscher Luft- und Raumfahrtkongress (DLRK)*; Deutsche Gesellschaft für Luft- und Raumfahrt, Ed.; DLRK: Rostock, Germany, 2015.
39. McCormick, B.W. *Aerodynamics, Aeronautics, and Flight Mechanics*, 2nd ed.; Wiley: Hoboken, NJ, USA, 1995; ISBN 0471110876.
40. Nita, M.; Scholz, D. *Aircraft Design Studies Based on the ATR 72*; Projektarbeit, HAW Hamburg: Hamburg, Germany, 2008.
41. Hosking, E.; Kenny, D.; McCormick, R.; Moustapha, S. The PW100 Engine: 20 Years of Gas Turbine Technology Evolution. In Proceedings of the RTO Meeting Proceedings, Utrecht, The Netherlands, 21–23 June 1999; pp. 4.1–4.9.
42. McKay, M.D.; Beckman, R.J.; Conover, W.J. A Comparison of Three Methods for Selecting Values of Input Variables in the Analysis of Output from a Computer Code. *Technometrics* **1979**, *21*, 239–245.

43. Seitz, A. Advanced Methods for Propulsion System Integration in Aircraft Conceptual Design. Ph.D. Thesis, Technische Universität München, Munich, Germany, 2012.
44. Hein, B. *UMD Atlas Design Proposal: Heavy Lift Helicopter*; UMD: College Park, MD, USA, 2005.
45. Kurzke, J. GasTurb 12—Design and Off-Design Performance of Gas Turbines, Germany. 2013. Available online: http://www.gasturb.de/Gtb12Manual/GasTurb12.pdf (accessed on 2 March 2019).
46. Filippone, A. *Advanced Aircraft Flight Performance*; Cambridge University Press: Cambridge, UK, 2013; ISBN 9781107024007.
47. Löbberding, H.; Wessel, S.; Offermanns, C.; Kehrer, M.; Rother, J.; Heimes, H.; Kampker, A. From Cell to Battery System in BEVs: Analysis of System Packing Efficiency and Cell Types. *WEVJ* **2020**, *11*, 77. [CrossRef]
48. Kellermann, H. Thermal Management Systems of Future Aircraft. Ph.D. Thesis, Technical University of Munich, Munich, Germany, 2023.
49. Viguier, C. IMOTHEP Internal Report RA5.2: Report on Static Optimized EPU Subsystem and Components along Requirements of Vehicle Designs L1. 2022. Available online: christophe.viguier2@safrangroup.com (accessed on 30 May 2023).
50. Cavallo, A.; Canciello, G.; Russo, A. Supervised Energy Management in Advanced Aircraft Applications. In Proceedings of the 2018 European Control Conference (ECC), Limassol, Cyprus, 12–15 June 2018; pp. 2769–2774.